LEVEL II

VPI-AERO-095

Numerical Prediction Of Flows Over And In The Near Wake Behind Axisymmetric, Self-Propelled Bodies

by

M. C. Hyman, S. C. Houlihan, J. A. Hill,
D. L. Dwoyer and C. H. Lewis

Department of Aerospace and Ocean Engineering
Virginia Polytechnic Institute and State University
Blacksburg, Virginia 24061

March 1979

(1)

(6) NUMERICAL PREDICTION OF FLOWS OVER AND IN THE NEAR WAKE BEHIND AXISYMMETRIC, SELF-PROPELLED BODIES,

by

(10) M. C./Hyman, S. C./Houlihan, J. A./Hill, D. L./Dwoyer and C. H./Lewis

(12) 71

Department of Aerospace and Ocean Engineering
Virginia Polytechnic Institute and State University
Blacksburg, Virginia 24061

(11) VPI-AERO 095

(11) Mar 1979

ABSTRACT

A technique is presented for the calculation of laminar, transitional and/or turbulent flows over and in the near wake behind bodies of revolution including the effects of separated flow and an operating propeller. The technique uses an interactive boundary-layer program to obtain a viscous solution over a nonseparating body and to provide upstream boundary conditions for a second program which solves the full Navier-Stokes equations for the propeller, separated flow and near wake regions.

The results of calculations made using individual elements of, and the complete system of codes were compared with good agreement against both experimental and numerical data and are included in the present work.

TABLE OF CONTENTS

ABSTRACT ii

LIST OF FIGURES iv

LIST OF TABLES vii

LIST OF SYMBOLS viii

INTRODUCTION 1

Interactive Boundary-Layer Solution Method 3

Wake Model 4

Propeller, Separated, and Wake Flows 4

ANALYSIS OF INTERACTIVE METHOD 6

Wake Calculations 8

Eddy Viscosity Laws 8

Transition Models 9

ANALYSIS OF NAVIER-STOKES EQUATIONS 11

RESULTS AND DISCUSSION 14

Long Cylinder Results 14

NSRDC Self-Propelled Body Data 15

COMPUTING TIME REQUIRED 18

CONCLUDING REMARKS 19

REFERENCES 20

LIST OF FIGURES

Figure		Page
1	Development and Effect of Wake Fairing Extension	24
2	Velocity Defect Profiles over Case 7 Cylinder	25
3	Velocity Profile over Case 7 Cylinder	26
4	Law of the Wall Profiles over a Case 7 Cylinder	27
5	Velocity Defect Profiles over Case 11 Cylinder	28
6	Comparison of Velocity Profiles over Case 11 Cylinder	29
7	Comparison of Law of the Wall Velocity Profiles over Case 11 Cylinder	30
8	Velocity Defect Profiles over a Case 14 Cylinder	31
9	Velocity Profile over a Case 14 Cylinder	32
10	Law of the Wall Velocity Profiles over a Case 14 Cylinder	33
11	Velocity Profiles of Test Case 1 Without a Propeller in Operation	34
12	Velocity Profiles of Test Case 1 Without a Propeller in Operation	35
13	Velocity Profiles of Test Case 1 Without a Propeller in Operation	36
14	Velocity Profiles of Test Case 1 Without a Propeller in Operation	37
15	Comparison of Pressure Distribution over Sumarine Model ($L_A/D = 4.307$)	38
16	Velocity Profiles of Test Case 2 Without a Propeller in Operation	39
17	Velocity Profiles for Test Case 2 Without a Propeller in Operation	40
18	Velocity Profiles for Test Case 2 Without a Propeller in Operation	41

LIST OF FIGURES (continued)

Figure		Page
19	Velocity Profiles of Test Case 1 with a Propeller in Operation	42
20	Velocity Profiles of Test Case 1 with a Propeller in Operation	43
21	Velocity Profiles of Test Case 1 with a Propeller in Operation	44
22	Velocity Profiles of Test Case 2 with a Propeller in Operation	45
23	Velocity Profiles of Test Case 2 with a Propeller in Operation	46
24	Velocity Profiles of Test Case 2 with a Propeller in Operation	47
25	Velocity Profiles in the Near Wake (X/L = 1.023) of Test Case 1 Without a Propeller in Operation	48
26	Velocity Profiles in the Near Wake (X/L = 1.05) of Test Case 1 Without a Propeller in Operation	49
27	Velocity Profiles in the Near Wake (X/L = 1.2) of Test Case 1 Without a Propeller in Operation	50
28	Velocity Profiles in the Near Wake (X/L = 1.4) of Test Case 1 Without a Propeller in Operation	51
29	Velocity Profiles in the Near Wake (X/L = 1.023) of Test Case 1 with a Propeller in Operation	52
30	Velocity Profiles in the Near Wake (X/L = 1.05) of Test Case 1 with a Propeller in Operation.	53
31	Velocity Profiles in the Near Wake (X/L = 1.2) of Test Case 1 with a Propeller in Operation	54
32	Velocity Profiles in the Near Wake (X/L = 1.4) of Test Case 1 with a Propeller in Operation	55
33	Velocity Profiles in the Near Wake (X/L = 1.0128) of Test Case 2 Without a Propeller in Operation	56

LIST OF FIGURES (continued)

Figure		Page
34	Velocity Profiles in the Near Wake (X/L = 1.18) of Test Case 2 Without a Propeller in Operation	57
35	Velocity Profiles in the Near Wake (X/L = 1.122) of Test Case 2 Without a Propeller in Operation	58
36	Velocity Profiles in the Near Wake (X/L = 1.00) of Test Case 2 with a Propeller in Operation	59
37	Velocity Profiles in the Near Wake (X/L = 1.0128) of Test Case 2 with a Propeller in Operation	60
38	Velocity Profiles in the Near Wake (X/L = 1.321) of Test Case 2 with a Propeller in Operation	61

LIST OF TABLES

Table		Page
1	Characteristics of Cylinder Test Cases	21
2	Characteristics of Submarine Test Cases	21
3	Comparison of Boundary-Layer Quantities of Case 7	22
4	Comparison of Boundary-Layer Quantities of Case 11	22
5	Comparison of Boundary-Layer Quantities of Case 14	23

LIST OF SYMBOLS (Boundary-Layer)

A	Constant in intermittency factor calculation
A_0	Constant in momentum equation
A_1	Constant in momentum equation
A_2	Constant in momentum equation
A_3	Constant in momentum equation
A_4	Constant in momentum equation
F	U/U_e nondimensional velocity distribution
j	Exponent in transformations
k	Exponent in transformations
n	Untransformed normal coordinate
r	Radial distance to boundary-layer point
r_w	Radial distance to wall at current profile
u	Axial velocity at boundary-layer point
U_e	Edge velocity
v	Normal velocity at boundary-layer point
x	Axial distance
β	$1/(j+1)$
ε	$Re^{-\frac{1}{4}}$ - Eddy viscosity
ε^+	ε/ν
ξ	Transformed surface coordinate
η	Transformed radial coordinate
κ	Longitudinal curvature
γ	Transition intermittency factor
$\bar{x}$	Length of transition region

LIST OF SYMBOLS (Navier-Stokes)

a_2	Constant in turbulence model
b	Mixing zone width
c_z	Constant in turbulence model
F_x	Thrust per unit area
H	Height of the region of solution
i	Counter in axial direction
j	Counter in radial direction
I_1, I_2	Integrals in TKE equation
k	Turbulence kinetic energy (TKE)
n	Index for time step
r	Radial coordinate
$\bar{r}$	r/b
t	Time
u	Axial velocity component
U_e	Edge velocity
$\bar{u}$	u/U_e
U_∞	Freestream velocity
v	Radial velocity component
x	Axial distance from the front of the region
ξ	Vorticity
ψ	Stream function
ε	Eddy viscosity
ρ	Density
τ	Shear
δ^*	Boundary-layer displacement thickness

INTRODUCTION

While considerable effort has been spent in obtaining experimental data in the wakes behind self-propelled bodies, somewhat less effort has been put into the prediction of the near wake. In the work that has been done, the method generally used is to calculate the flow about the body and utilize this as a basis for a wake solution.

Several studies have attempted to obtain solutions of the flowfield about the body with the inclusion of viscous effects. The usual method is to use some initial pressure distribution as a first guess and then make use of boundary-layer theory over the forebody and non-separating sections of the afterbody. The boundary-layer solutions obtained are used by adding the displacement thickness from the boundary-layer solution to the original body and, in turn, employing the new body in calculating a new pressure distribution. The sequence is continued in the same manner until a convergence is met by specifying that the displaced body not change more than some amount between iterations. The methods differ in their approach to the treatment of the separated region, the stern, near-wake and far-wake regions.

Beatty[1] adds the displacement thickness found through a boundary-layer solution to the original body up to the trailing edge. This procedure yields a cylindrical body with an abrupt, open end. Wake solutions are found by extending a tube with radius of the displaced body at the trailing edge and calculating an inviscid solution over this tube. The body/tube joint is accomplished by fairing a circular arc, tangent to the body and tube. The method of Cebeci, Mosinskes and Smith[2] simply

INTRODUCTION

While considerable effort has been spent in obtaining experimental data in the wakes behind self-propelled bodies, somewhat less effort has been put into the prediction of the near wake. In the work that has been done, the method generally used is to calculate the flow about the body and utilize this as a basis for a wake solution.

Several studies have attempted to obtain solutions of the flowfield about the body with the inclusion of viscous effects. The usual method is to use some initial pressure distribution as a first guess and then make use of boundary-layer theory over the forebody and non-separating sections of the afterbody. The boundary-layer solutions obtained are used by adding the displacement thickness from the boundary-layer solution to the original body and, in turn, employing the new body in calculating a new pressure distribution. The sequence is continued in the same manner until a convergence is met by specifying that the displaced body not change more than some amount between iterations. The methods differ in their approach to the treatment of the separated region, the stern, near-wake and far-wake regions.

Beatty[1] adds the displacement thickness found through a boundary-layer solution to the original body up to the trailing edge. This procedure yields a cylindrical body with an abrupt, open end. Wake solutions are found by extending a tube with radius of the displaced body at the trailing edge and calculating an inviscid solution over this tube. The body/tube joint is accomplished by fairing a circular arc, tangent to the body and tube. The method of Cebeci, Mosinskes and Smith[2] simply

modifies the body by adding the displacement thickness to the original body up to the trailing edge; however, no model of the wake is suggested.

Nakayama[3] employs a more complex model. A boundary-layer solution is found over the forebody and the far wake, but Nakayama does not use the displacement thickness for body modification. The potential flow solution is matched at the edge of the boundary layer and wake. Also a transverse pressure gradient is used in the boundary-layer in the near wake.

The method of Brune, Ruppert and Forester[4] uses a boundary-layer solution over the forebody and a complete Navier-Stokes solution of the afterbody and into the wake. The method, however, is limited to treatment of laminar flow. The use of the Navier-Stokes equations over so large a body section requires extensive computational time.

Huang, Wang, Santelli and Groves[5] employed a boundary-layer solution over the body and into the wake using the displacement thickness to modify the body. In the separated region, a polynomial fairing was used to approximate the displacement thickness from the separation point on the body to some point in the wake. The globally interative scheme was continued until convergence was met. A propeller calculation was performed using a propeller field-point program and a pressure calculation due to the propeller presence. The results were compared with experimental data with good agreement; however, no wake calculations were given.

Recently Schetz and Favin[6] developed a Navier-Stokes code to predict the propeller region of a self-propelled body. We have developed a complete flowfield prediction code which embeds the Schetz-Favin Navier-

Stokes code in an inviscid outer flow and coupled boundary-layer flowfield to predict the upstream boundary conditions, the initial estimate of the flowfield within the Navier-Stokes region and the downstream near wake region. For the nonseparating, nonpropelled body, only the interacting boundary-layer code is needed.

Interactive Boundary-Layer Solution Method

The current method uses a boundary-layer solution with the edge conditions matched to those given by a first estimate potential flow distribution obtained through the Hess 2-D and Axisymmetric Potential Flow Program.[7] The boundary-layer displacement thickness is added to the body to generate a displacement body about which a new inviscid pressure distribution is found. In the trailing edge region, separated flow is approximated by a fairing of the body into the wake beginning at a point above the separated region. Construction of the fairing is accomplished through an iterative procedure by locating the separated region using a potential flow calculation, fixing a set of end points and recalculating the potential flow solution. The fairing is adjusted on each iteration until the inviscid pressure distribution indicates that the flow is nonseparating. The criterion for an inviscid indication of separation was determined through trial and error using the boundary-layer solution and is valid for all bodies. The flow about the fairing is assumed to be similar to that of an attached flow. The trailing edge region is thus "transformed" from a separating region to a nonseparating region. The solution is iterated until some convergence criterion is met.

Wake Model

The wake is modeled by first approximating it as a zero thickness body and assuming that the initial pressure distribution along the wake is that of the pressure on the afterbody. Thus the wake is modeled in a manner which allows a solution to proceed along with the body.

Propeller, Separated, and Wake Flows

Propeller, separated, and near-wake flows are treated using the full Navier-Stokes equations. The region of solution extends from a point on the body forward of the separated region to some point in the wake. The location of these end points is the result of two considerations. First, the upstream boundary should be sufficiently forward of the point of separation and the propeller so that the effects of each of these may be included in the calculations. Second, a constant axial stepsize is used in the region of solution. The x-stepsize is determined by the location of the upstream boundary since a specific number of points must be placed on the body to obtain a solution with sufficient resolution.

The Navier-Stokes equations require boundary conditions all around the closed region of interest, and the specific formulation used in the present study requires additionally an initial estimate of the stream function throughout the region of solution. Upstream conditions include both viscous boundary layer and inviscid outer flow regions. The conditions in the viscous region are supplied by the iterated boundary-layer solution in the form of velocity profiles. Conditions in the inviscid region are obtained by calculating the inviscid flowfield about

the displaced body. Likewise the initial estimate of the stream function is given by the flowfield about the displaced body. The upper boundary conditions are taken as the velocities from the initial stream function. It is therefore required that the upper boundary be placed sufficiently far from the body to insure that the effects of the propeller and separated flow be negligible. By studying the results of numerous test cases it was found that for all bodies considered, the upper boundary was indeed far enough removed from the body using the normal stepsize which accompanies the axial stepsize (the two stepsizes are directly related). Finally the downstream conditions are that both $\partial^2\xi/\partial x^2$ and $\partial^2\psi/\partial x^2$ vanish along this boundary.

ANALYSIS OF INTERACTIVE METHOD

The boundary-layer solution is obtained through the use of basic incompressible boundary-layer theory, valid for laminar and turbulent flow with appropriate boundary conditions for wake calculations. The laminar boundary-layer equations with transverse curvature effects included[8] are as follows:

$$(r^j u)_x + (hr^j v)_n = 0$$

$$uu_x + v(hu)_n = -p_x + \frac{h}{r^j}\left[\frac{r^j}{h^j}(hu)_n\right]_n$$

where

$$r = r_0 + \varepsilon n\cos\phi$$

$$h = 1 + \varepsilon\kappa n$$

$$\varepsilon = R_e^{-\frac{1}{2}}$$

To make the wake calculations, the conventional Levy-Lees transformation was foregone as it is incapable of handling a sharp trailing edge and body of zero radius. (The wake is represented as a body-point, coordinates (x,0).) Therefore, the boundary-layer equations were transformed using a variation of the Levy-Lees.

$$\xi = \int_0^x U_e r_w^{2j} U_e^{2k}\, dx$$

$$n = \int_0^n \frac{U_e}{\sqrt{2\xi}}\, r^{j+k}\, dn$$

where $j = 1$ for 2-D flow and 2 for axisymmetric flow and $k = 1$ for body only flow and 2 for wake flow. This transformation eliminates both

stagnation point and sharp trailing edge singularities; however, it is not a similarity transformation and thus requires that the grid system be adjusted as the solution progresses to accommodate the growth of the boundary layer.

The use of the new transformation yields equations of the same form as those obtained through the Levy-Lees transformation.

With the definition $F = u/U_e$ and $\varepsilon^+ = \varepsilon/\nu$ the momentum equation becomes:

$$F_{\eta\eta} + A_1 F_\eta + A_2 F + A_3 + A_4 F_\xi = 0$$

$$A_1 = [(A_0)_\eta - V]/A_0$$

$$A_2 = -\beta F/A_0$$

$$A_3 = \beta/A_0$$

$$A_4 = -2\xi F/A_0$$

$$A_0 = r^{2j}(1 + \varepsilon^+)/r_w$$

The method of solution involves using an initial velocity profile as a guess and solving the momentum equation. The initial guesses used are solutions from the previous iteration. On the initial iteration on a profile the converged solution of the previous station profile is used. At the stagnation point a removable singularity exists and the boundary-layer equations become at $\xi = 0$:

$$F + V_\eta = 0$$

$$V + F_\eta + (j+1)^{-1}(F^2-1) = [(r/r_w)^{2j}(1+\varepsilon^+)F\eta]_\eta$$

with additional boundary conditions from the edge velocity. The solution at the stagnation point yields a starting solution for the marching procedure to begin.

Wake Calculations

In extending the solution into the wake, the same boundary-layer equations are employed as on the solid body, now subject to the symmetry boundary condition, $F'(x,0) = 0$. The solution is then obtained as before. For each case (axisymmetric, 2-D, wake, and no wake) the calculation is begun at the leading edge and continued along the length of the body so that no discontinuities will exist.

Eddy Viscosity Laws

For turbulent (and transition) flows, the Reynolds shear term is given by a two-layer eddy viscosity model. Two different equations are used for the eddy viscosity. One equation (referred to as the inner law) is used in the region of the boundary layer near the wall, the other equation (the outer law) is used in the outer region of the boundary layer. The inner region extends from the wall to the point where the eddy viscosity for the inner and outer laws are equal. The center region extends from the matching point to the edge of the boundary layer. The outer law, which follows Clauser's work using Klebanoff's intermittency factor, gives values which tend to zero at the outer edge of the boundary layer. The program provides the user with two choices for the inner eddy viscosity law. One follows the work of Van Driest, the other is the eddy viscosity law derived by Reichardt. In general, the results obtained from the program using both laws have been equivalent, although the

calculations using the Reichardt law required less computing time, and therefore, the Reichardt law is recommended for most applications.

Transition Models

Two transition models have been included for use in the boundary-layer solution. Satisfactory agreement has been obtained with experimental results for several cases involving transition, but only by selecting appropriate values of the transition parameters CHICRT and XBAR. Calculations involving transition are most satisfactory when done ex post facto; that is, when the parameters can be appropriately adjusted to obtain agreement with the experimental results.

The first transition model changes the flow instantaneously from laminar to turbulent at a specified axial position and then reduces the axial stepsize.

The second transition model provides a regime of transition from laminar to turbulent flow. The calculation is started with the flow laminar ($\varepsilon^+=0$), and at the beginning of transition, the flow is changed to turbulent with the eddy viscosity attenuated by the transition intermittency factor. The intermittency factor increases from zero to unity as $\bar{x}$ increases, and the eddy viscosity reaches its fully turbulent value at some distance downstream of the point where transition begins.

The procedure which is used to indicate the beginning of transition utilizes the vorticity Reynolds number which is given by the following expression:

$$\chi = \frac{y^2}{\nu} \frac{\partial u}{\partial y}$$

Transition is initiated when the maximum value of χ, χ_{max} exceeds a critical value, χ_{crit}(=CHICRT), which is generally in the range of 2000 to 4000.

The transition intermittency factor is given by the expression

$$\Gamma = 1 - \exp(-A\bar{\xi}^2)$$

where $A = 0.412$ and $\bar{\xi} = (\chi - \chi_0)/\lambda$.

The value of χ at the beginning of transition is χ_0 and λ is a measure of the length of the transition region which is given by Owen (1970) as $\lambda = \chi_{\Gamma=3/4} - \chi_{\Gamma=1/4}$.

The values of χ needed to calculate λ cannot be predetermined and an equivalent expression for λ is used instead with λ given by the expression $\lambda = \chi_0(\bar{x}-1)/4$ where $\bar{x}$(=XBAR) is another measure of the length of transition which is such that $\chi_{\text{end of transition}} = \bar{x}\ \chi_{\text{beginning of transition}}$. When the Van Driest inner eddy viscosity law is used, the above expression is quite close to an exact equality. For calculations with the Reichardt inner eddy viscosity law equivalent results are obtained when $\bar{x}$ is increased by about 65 percent. Then, however, the above expression misses equality by 65 percent. With the Van Driest inner eddy viscosity law, 2.0 has been found to be an appropriate value for XBAR for some cases and larger values of XBAR have been required to obtain reasonable agreement with experimental results in other cases. The values of CHICRT and XBAR cited above should provide reasonable initial estimates of appropriate values of these parameters.

ANALYSIS OF NAVIER-STOKES EQUATIONS

The Navier-Stokes equations are used to generate the near wake behind the body and include the effects of separated flow.[6]

An actuator disk provides a momentum increase to the flow which simulates propeller effects for the wake region.

The full Navier-Stokes equations along with the definition of vorticity for the above inclusions are:

$$\frac{\partial \xi}{\partial t} + u\frac{\partial \xi}{\partial x} + v\frac{\partial \xi}{\partial y} - \frac{v\xi}{r} = \varepsilon\left[\frac{\partial^2 \xi}{\partial r^2} + \frac{1}{r}\frac{\partial \xi}{\partial r} + \frac{\partial^2 \xi}{\partial x^2} - \frac{\xi}{r^2} + \frac{1}{\rho}\frac{\partial F_x}{\partial r}\right] \quad (1)$$

and

$$r\xi = \frac{\partial^2 \psi}{\partial r^2} + \frac{\partial^2 \psi}{\partial x^2} - \frac{1}{r}\frac{\partial \psi}{\partial r} \quad (2)$$

From the above stream function, the u and v velocity components can be obtained by $ur = \partial\psi/\partial r$ and $vr = -\partial\psi/\partial x$ (3)

As shown in Fig. 1, the boundary conditions are as follows:

$$u(0,r) = U_0(r)$$

$$v(0,r) = V_0(r)$$

$$\xi(x,H) = 0 \quad (4)$$

$$\psi(x,H) = \psi(x,H-\Delta r) + U_e(x)\Delta r$$

At the downstream boundary, the following conditions are specified

$$\partial^2\psi/\partial x^2 = 0 \text{ and } \partial^2\xi/\partial x^2 = 0 \quad (5)$$

Along the solid body

$$\psi(x,r_w) = 0, \quad u_b = 0, \quad v_b = 0 \quad (6)$$

and finally in the wake,

$$\psi(x,0) = 0, \quad \xi(x,0) = 0 \quad (7)$$

Using a third-order Taylor series expansion, the stream function near the wall is

$$\psi(x,r_b+\Delta r) = \psi_b + \Delta r\partial\psi/\partial r + (\Delta r)^2\partial^2\psi/\partial r^2 + (\Delta r)^3\partial^3\psi/\partial r^3 + \ldots \quad (8)$$

Similarly,

$$\psi(x+\Delta x,r_b) = \psi_b + \Delta x\partial\psi/\partial x + (\Delta x)^2\partial^2\psi/\partial x^2 + (\Delta x)^3\partial^3\psi/\partial x^3 + \ldots \quad (9)$$

Since $u(r_w) = 0$ and $v(r_w) = 0$, $\psi_b = 0$. Using these results, the vorticity at the wall becomes

$$\xi_b = \left(\frac{\partial u}{\partial r} - \frac{\partial v}{\partial x}\right) r_b = \frac{2}{r_b}\left[\frac{\psi(x+\Delta x,r_b)}{(\Delta x)^2} + \frac{\psi(x,r_b+\Delta r)}{(\Delta r)^2}\right] \quad (10)$$

At the tail of the body r_b approaches zero so a modified vorticity equation is used.

$$\xi_b = 3\psi(x,\Delta r)/(\Delta r)^3 \quad (11)$$

An initial flowfield is set up by reading in the displaced, inviscid velocity field. The velocity field is then used to generate a stream function as follows:

$$\psi_j = \psi_{j-1} + \frac{\Delta r}{2}(u_j r_j + u_{j-1} r_{j-1}) \quad (12)$$

For an axisymmetric body the integrated turbulent kinetic energy equation is

$$\int_0^{b(x)} \frac{\partial \rho u}{\partial x} r\,dr = \int_0^{b(x)} \frac{\partial u}{\partial r} \tau r\,dr - \frac{a_z}{b} \int_0^{b(x)} \rho k^{2/3} r\,dr \quad (13)$$

Defining an eddy viscosity and following Prandtl's model

$$\tau = \rho\varepsilon\partial u/\partial r = \rho k^{1/2} L\partial u/\partial r \quad (14)$$

With $L = c_2 b$, $\bar{u} = u/U_e$, and $\bar{r} = r/b$, the TKE equation may be written

$$\frac{d\varepsilon(x)}{dx} = \frac{c_2 U_e}{2}\left[\frac{I_2}{I_1}\right] - \frac{a_2\varepsilon^2}{4U_e c_2 b_2 I_1} - \frac{\varepsilon}{2I_1}\frac{dI_1}{dx} + \frac{\varepsilon}{2b}\frac{db}{dx} - \frac{\varepsilon}{2U_e}\frac{dU_e}{dx} \quad (15)$$

with

$$I_1(x) = \int_0^1 \bar{u}\bar{r}d\bar{r} \text{ and } I_2(x) = \int_0^1 (\partial\bar{u}/\partial\bar{r})^2\bar{r}d\bar{r} \quad (16)$$

To model tip losses from an actual propeller in the actuator zone, the following analysis is used. For the five points near the upper edge of the actuator zone, the force provided is defined by

$$\frac{F_x}{\rho} = \frac{F_{x_0}}{2}\left\{1 + \cos\left[\frac{\pi[r-(L1-5)\Delta r]}{4\Delta r}\right]\right\} \quad (17)$$

Elsewhere in the actuator zone

$$F_x/\rho = F_{x_0} = \text{constant} \quad (18)$$

where F_{x_0} is determined by a momentum loss caused by the boundary layer defect.

The eddy viscosity is defined by

$$\varepsilon = 0.0168\delta^* U_e \quad (19)$$

where

$$(\delta^*)^2 = \int_0^\delta \left(1 - \frac{u}{U_e}\right) r dr \quad (20)$$

RESULTS AND DISCUSSION

In the present work the principle interest is in the near wake predictions with and without both separated flow and an operating propeller. Because of the modular solution procedure, the interactive boundary-layer solution and Navier-Stokes solution, it is desired to compare the predictions of each section with both numerical and experimental data. Predictions of the near wake regions obtained through the use of the complete procedure are then given.

Long Cylinder Results

Interactive boundary-layer/potential flow predictions were compared to the measurements of Wilmarth.[8] In this study, long, small diameter cylinders were employed to develop thick, turbulent boundary layers. A total of three cases were chosen for comparison purposes. These cases reflect the effects of increasing the cylinder diameter and consequently varying the degree of transverse curvature. Table 1 gives the various physical descriptions of the cases under consideration. Figures 2 and 3 give comparisons of the u/u^+ profiles and velocity defect profiles for Wilmarth's case 7. Figures 2 and 3 show excellent agreement over the entire boundary-layer, while Fig. 4, giving a comparison of the Law of the Wall velocity profile for the same case, shows a poorer but still good agreement.

Figures 5, 6, and 7 give the corresponding profiles for case 11 which is a larger diameter cylinder at a higher freestream velocity. Again, agreement in the comparisons of velocity profiles and velocity defect profiles is good with maximum error occuring between the 20 and

40 percent of the boundary-layer thickness. This error may be attributed to the constants used in the eddy-viscosity model where the inner and outer law models are joined. Evidence of this is seen in the Law of the Wall profile where maximum error, while very small, is found at the extreme edge of the inner law region.

Figures 8, 9, and 10 show comparison profiles for the case 14 cylinder. In Figs. 8 and 9, very good agreement is shown and general behavior is much like that of the previous case. The difference in the slope of the measured and computed profiles is reflected in the tabulation of boundary-layer quantities for this case found in Table 5. In Fig. 10, showing the comparison of the Law of the Wall profile for this case, the meeting of the two eddy viscosity laws is seen to have a more localized impact, at the extreme edges of their regions of application.

Tabulated data giving the comparison and percent error of the boundary-layer quantities: displacement thickness, boundary-layer thickness, momentum thickness, friction velocity and friction coefficient are found in Tables 3, 4, and 5.

NSRDC Self-Propelled Body Data

Further comparisons of both the interactive boundary-layer procedure results and the results obtained from the entire system were made against the measured and calculated results obtained by the David W. Taylor Naval Ship Research and Development Center[5] for a body of revolution with and without the effect of an operating propeller. Several cases were considered, each consisting of a submarine like hull with varying degrees of taper in the afterbody. Of the three treated in the

original work, two were employed for comparison with the present method. Data describing the bodies are given in Table 2.

Figures 11 through 14 show velocity profiles on the aft portion of body 1 without an operating propeller. Agreement with experimental data is good. At body location X/L = 0.915 deviations from the numerical results are significant, showing a less turbulent profile than NSRDC predictions. At X/L = 0.971, the current method predicts a more turbulent flow than both experimental and numerical results of NSRDC. Figure 15 shows the pressure distribution over afterbody 1, and the prediction is in good agreement with experimental values.

Figures 16 through 18 show the predictions obtained for afterbody 2 without an operating propeller. Agreement is good at position X/L = 0.935 but deteriorates rapidly further aft. It should be noted that the boundary-layer procedure predicted a flow near separation. On the initial iterations the C_p distribution indicated a separating flow so that the body required modification to approximate the separated region. The result is the prediction of an extremely turbulent flow.

Figures 19 through 21 show comparisons of experimental and numerical data of Ref. 5 for afterbody 1 against predictions of the Navier-Stokes solution for on-body points with propeller. Agreement is fair, with the exception of the most upstream station where a somewhat more laminar flow is predicted than exists. This trend is accentuated as the solution progresses down the body.

Figures 22 through 24 give the velocity profiles over afterbody 2 with an operating propeller. Agreement is fair for X/L = 0.935 but deteriorates as the solution approaches the propeller region. Navier-

Stokes solutions in general show an extremely pronounced propeller effect on the flow.

Figures 25 through 28 show the wake predictions obtained through the interactive boundary-layer procedure and those obtained through the Navier-Stokes solution at progressively greater distances downstream of the body. Agreement between the two is poor and at the most distant profile considered, at X/L=1.40, the wake has effectively disappeared. This result is expected, though inaccurate. The procedure requires that 15 grid points of 60 be placed on the body for sufficient accuracy of the solution. However, in doing so, the x grid stepsize and hence the location of the downstream edge of the region of solution is thus defined. For the bodies under consideration, this requirement placed the region end at an essentially near wake location. This situation violates the downstream boundary conditions which are far wake conditions, and the effects of this violation are clearly seen.

Figures 29 through 32 show results for case 1 including the effects of a propeller while Figs. 23 through 38 show the predicted wake flows for case 2 with and without an operating propeller.

COMPUTING TIME REQUIRED

Computing time required with the IBM 370/158 computer using the G compiler for executing the long cylinder predictions were approximately 5.5 minutes for each iteration of the interactive boundary-layer procedure. The execution of the interactive boundary-layer solution corresponding to the submarine bodies used in Ref. 5 required approximately 8.5 minutes for the initial boundary-layer solution iteration and 2.0 minutes for subsequent iterations with the restart option. Restart was performed along the approximately cylindrical middle section of the body. Execution time for the Hess Potential Flow Program is approximately 40 seconds using 100 points for body description. Execution time when off-body flow properties are desired increases the execution time by approximately 50 seconds for 360 off-body points. Navier-Stokes solutions require approximately 6.0 minutes for no propeller cases and an additional 90 seconds when a propeller is included.

CONCLUDING REMARKS

The comparison of the results of the boundary-layer procedure against those experimental data of Ref. 8 was intended to establish the capability of the procedure. The agreement shown in the above analysis attests to this capability, and the demonstrated accuracy indicates that the procedure could be relied upon in further treatment of other bodies.

The results of both the present interactive boundary-layer procedure and Navier-Stokes solution procedure were compared to other numerical and experimental results. Agreement of the interactive procedure is, in general, good, while predictions of the complete system were poorer. It is felt that if the region treated by the Navier-Stokes solution procedure is extended far enough downstream to make the use of far wake boundary conditions more appropriate, the results of such computations will reflect a more realistic wake solution. This extension will increase computational time approximately as the square of the array size describing the Navier-Stokes region.

REFERENCES

1. Beatty, T.D., "A Theoretical Method for the Analysis and Design of Axisymmetric Bodies," NASA CR-2498 (1975).

2. Cebeci, T. et al., "Calculation of Viscous Drag and Turbulent Boundary Layer Separation of Two-Dimensional and Axisymmetric Bodies in Incompressible Flows," Douglas Aircraft Report MDC J0973-01 (1970).

3. Nakayama, A., "Viscid-Inviscid Interaction Due to the Thick Boundary Layer near the Tail of a Body of Revolution," PhD Thesis, University of Iowa (1974).

4. Brune, G.W. et al., "The Analysis of Flow Fields with Separation by Numerical Matching," Symposium on Flow Separation, Advisory Group for Aerospace Research and Development, Germany (1975).

5. Huang, T.T. et al., "Propeller/Stern/Boundary-Layer Interaction on Axisymmetric Bodies: Theory and Experiment," David W. Taylor Naval Ship Research and Development Center, Report 76-0113 (1976).

6. Schetz, J.A. and Favin, S., "Numerical Solution for the Near Wake of a Body with Propeller," Journal of Hydronautics, October 1977, Vol. 11, No. 4, pp. 136-144.

7. Davis, R.T., Whitehead, R.E. and Wornom, S.F., "The Development of an Incompressible Boundary-Layer Theory Valid to Second Order." VPI&SU College of Engineering, VPI-E-70-1, Blacksburg, Virginia, January 1970.

8. Wilmarth, W.W. et al., "Axially Symmetric Turbulent Boundary Layers on Cylinders: Mean Velocity Profiles and Wall Pressure Fluctuations," University of Michigan Report, No. 021490-3-T, University of Michigan, Ann Arbor, Michigan, June 1975.

TABLE I. CHARACTERISTICS OF CYLINDER TEST CASES[1]

	Case 7	Case 11	Case 14
Dia.	0.250	0.500	2.000
V_∞	160	192	204
Ra^2	9494	23100	92310
Re_θ	1.44×10^4	1.42×10^4	2.16×10^4

[1] Length for all cases: 18.3 ft.

[2] $Ra = Ud/2\nu$, d = diameter

TABLE II. CHARACTERISTICS OF SUBMARINE TEST CASES

	Case 1, N.P.[1]	Case 1, W.P.[2]	Case 2, N.P.[1]	Case 2, W.P.[2]
L^3/D	10.975	10.975	10.975	10.975
La^4/D	4.3078	4.3078	2.2472	2.2472
Le^5/D	0.4	0.4	0.4	0.4
V_∞	100.00	100.00	100.00	100.00
Re	5.9×10^6	5.9×10^6	5.9×10^6	5.9×10^6

[1] No propeller

[2] With propeller

[3] L = overall length

[4] La = length of afterbody

[5] Le = length of forebody

TABLE III. COMPARISON OF BOUNDARY-LAYER QUANTITIES OF CASE 7

Quantity	Data of Wilmarth	Boundary-Layer Calculation	% Error
δ (ft)	0.0984	0.0732	25.60
δ^* (ft)	0.0171	0.0119	32.2
θ (ft)	0.0158	0.0109	31.01
u^+ (ft/sec)	6.5500	7.0747	-8.01
C_f	3.34×10^{-3}	3.9077×10^{-3}	-16.99

TABLE IV. COMPARISON OF BOUNDAYR-LAYER QUANTITIES OF CASE 11

Quantity	Data of Wilmarth	Boundary-Layer Calculation	% Error
δ (ft)	0.0965	0.0778	19.84
δ^* (ft)	0.0142	0.0127	10.56
θ (ft)	0.0128	0.01125	12.10
u^+ (ft/sec)	7.4087	7.811	-5.43
C_f	2.98×10^{-3}	3.310×10^{-3}	-11.07

TABLE V. COMPARISON OF BOUNDARY-LAYER QUANTITIES OF CASE 14

Quantity	Data of Wilmarth	Boundary-Layer Calculation	% Error
δ (ft)	0.1566	0.1184	32.26
δ^* (ft)	0.0245	0.0198	23.73
θ (ft)	0.0195	0.0167	16.76
u^+ (ft/sec)	6.979	7.546	-7.52
C_f	2.34×10^{-3}	2.63×10^{-3}	-11.02

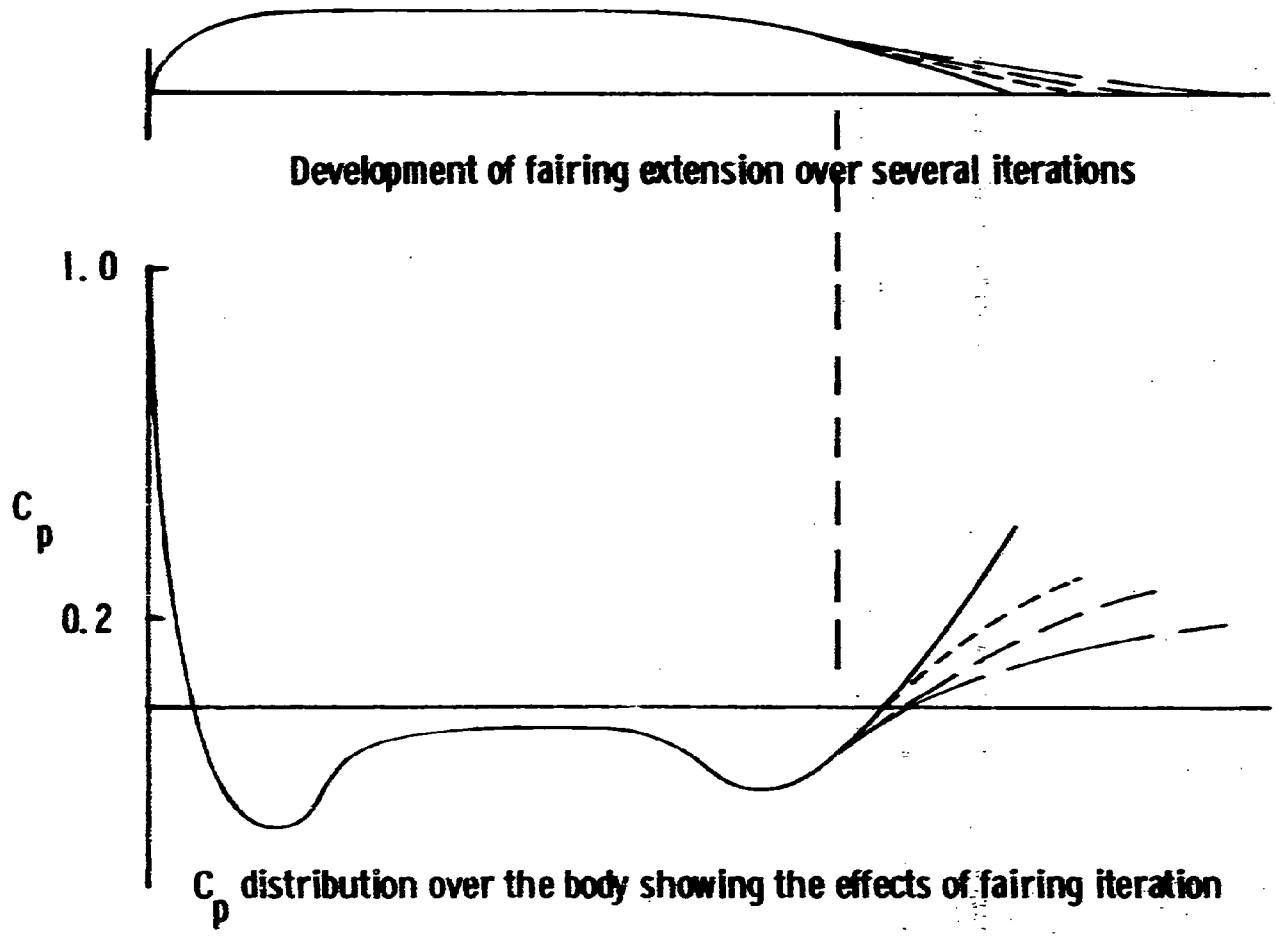

Fig. 1 Development and effect of wake fairing extension

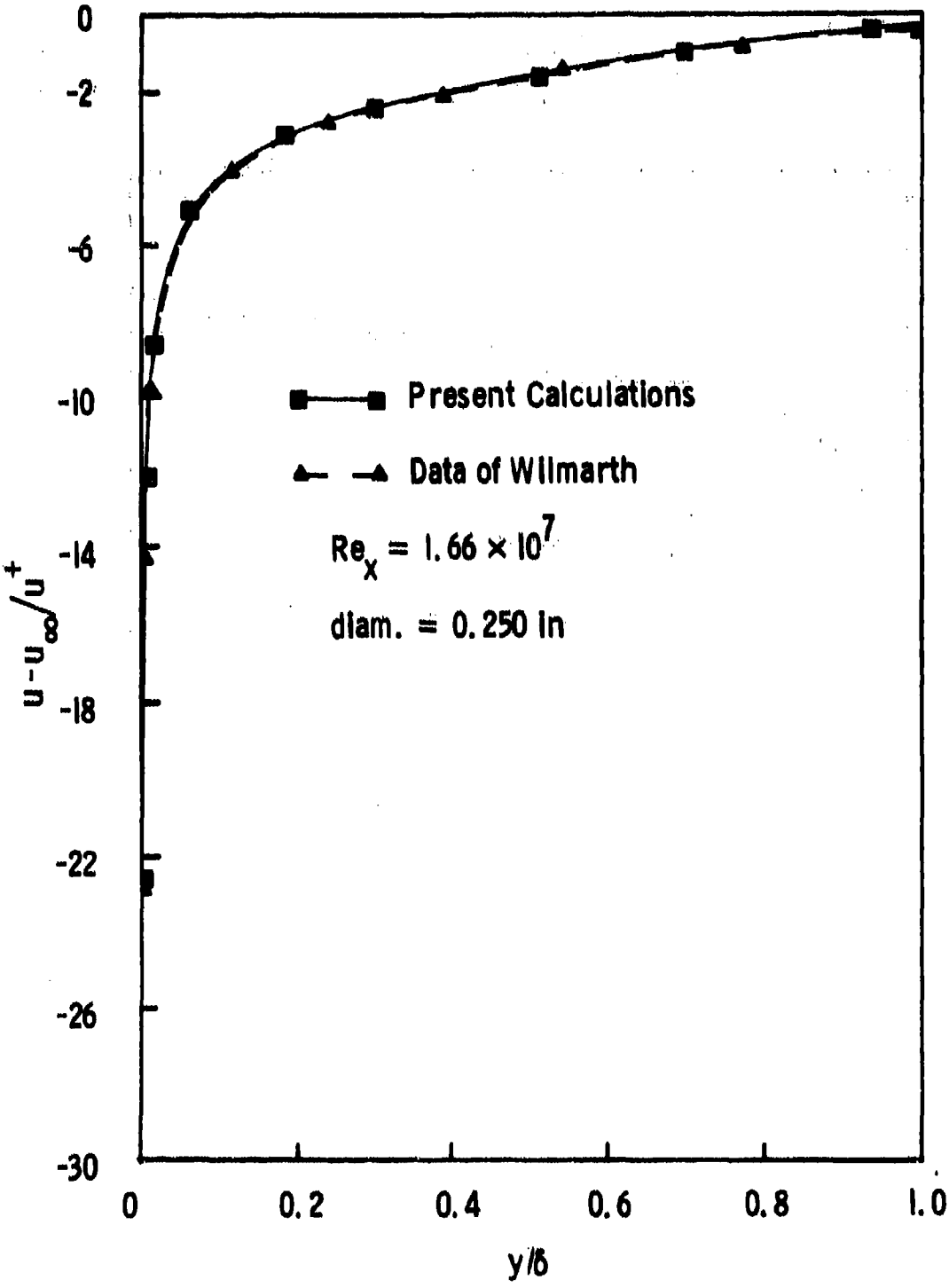

Fig. 2 Velocity defect profiles over case 7 cylinder

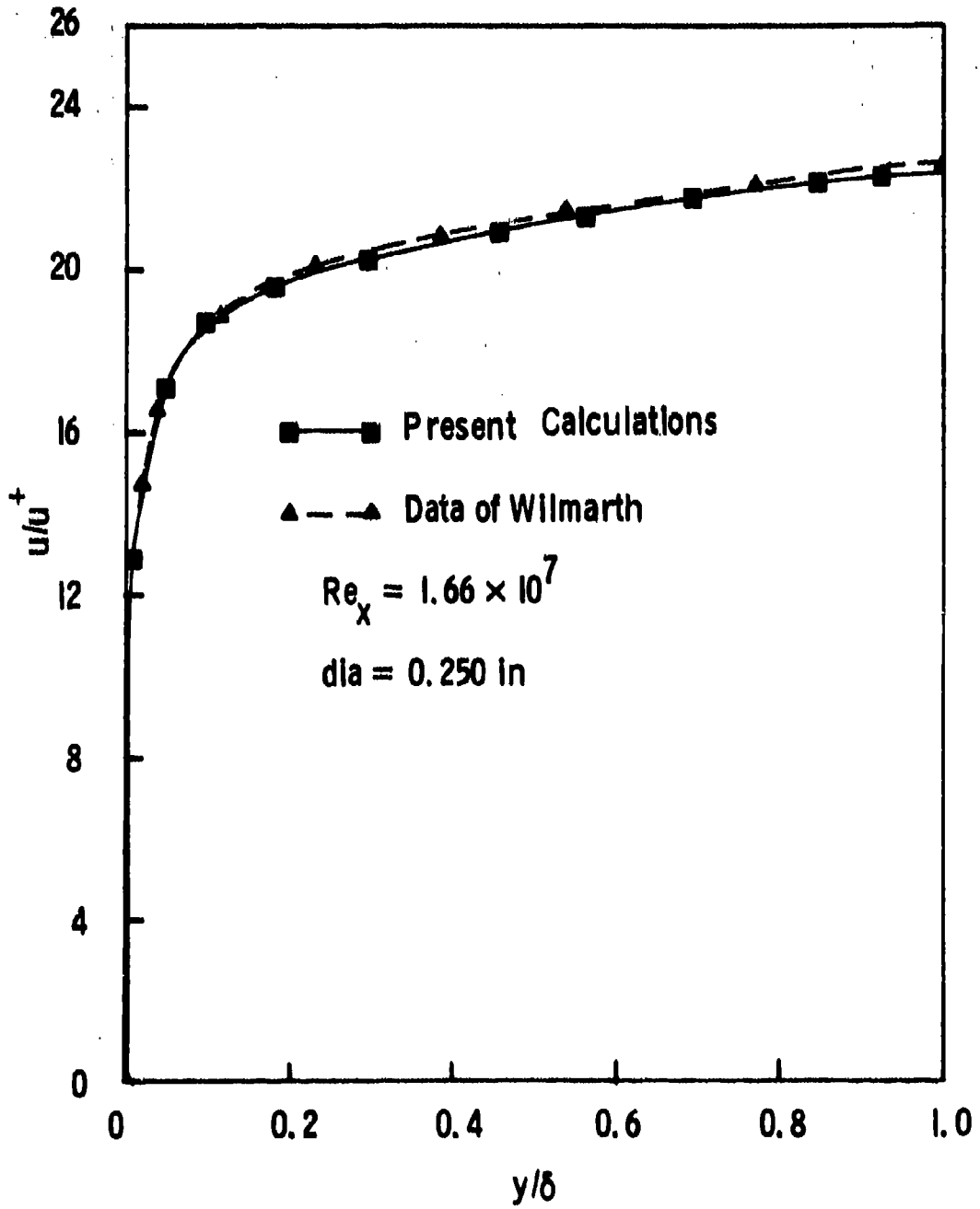

Fig. 3 Velocity profile over case 7 cylinder

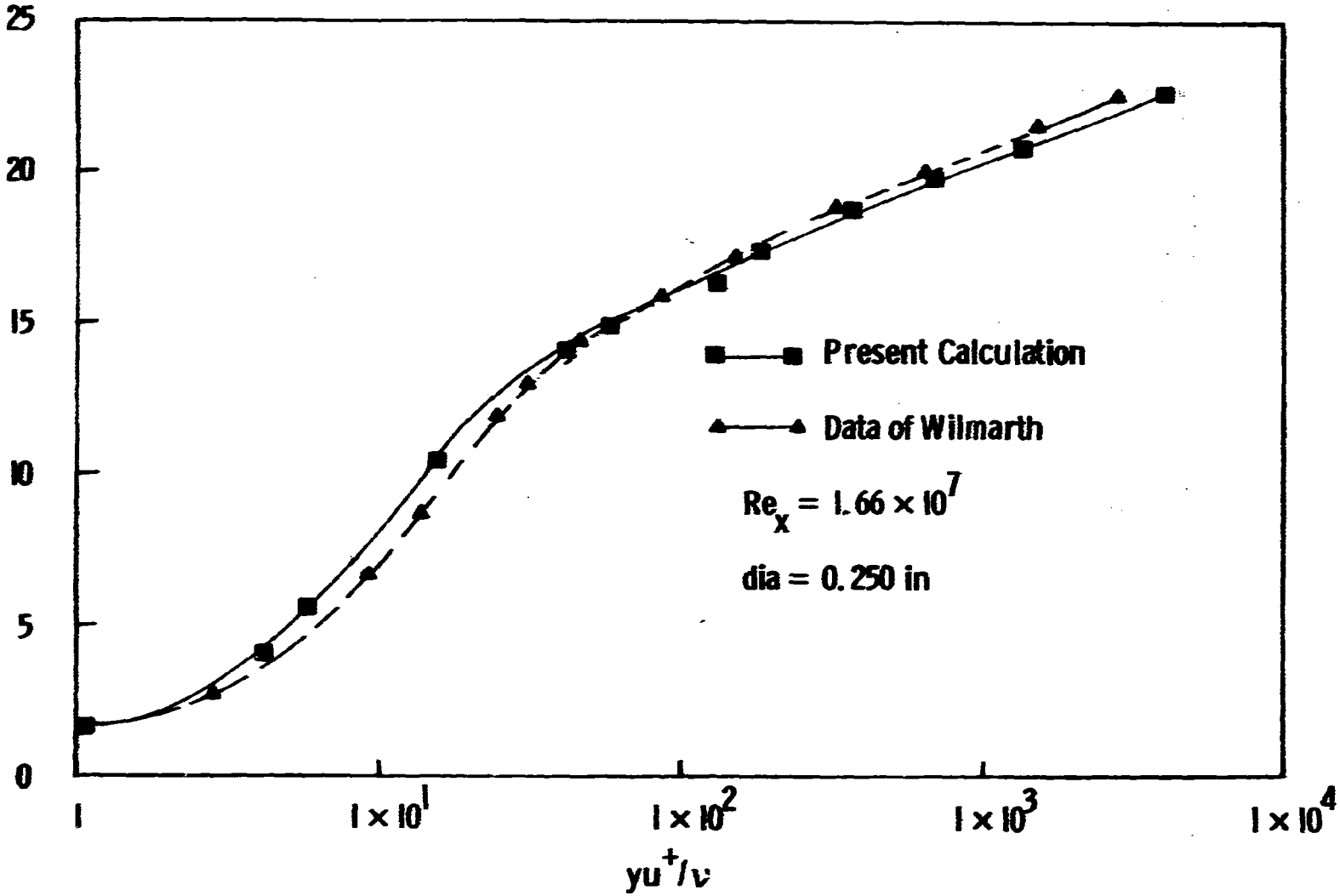

Fig. 4 Law of the wall profiles over a case 7 cylinder

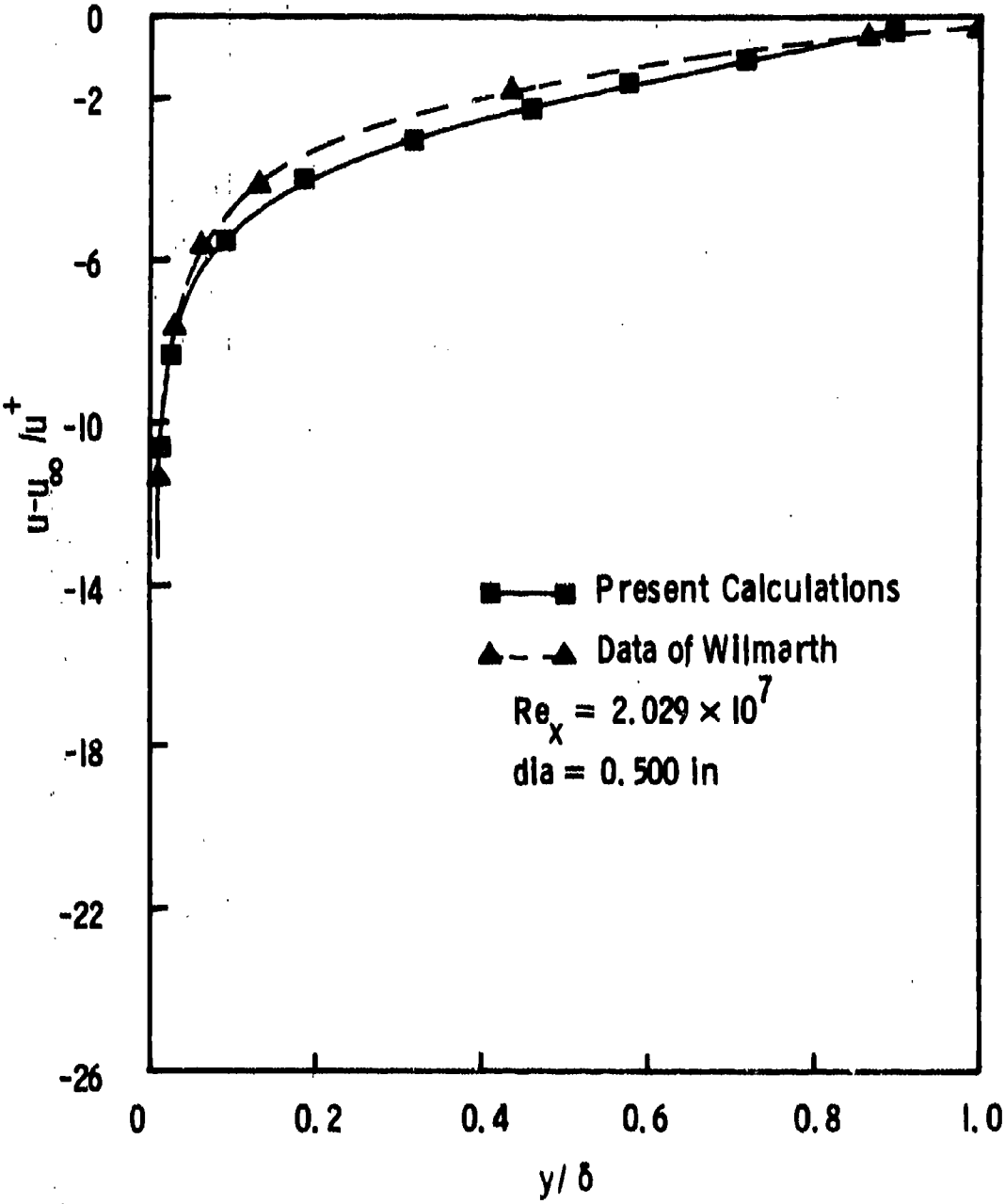

Fig. 5 Velocity defect profiles over case II cylinder

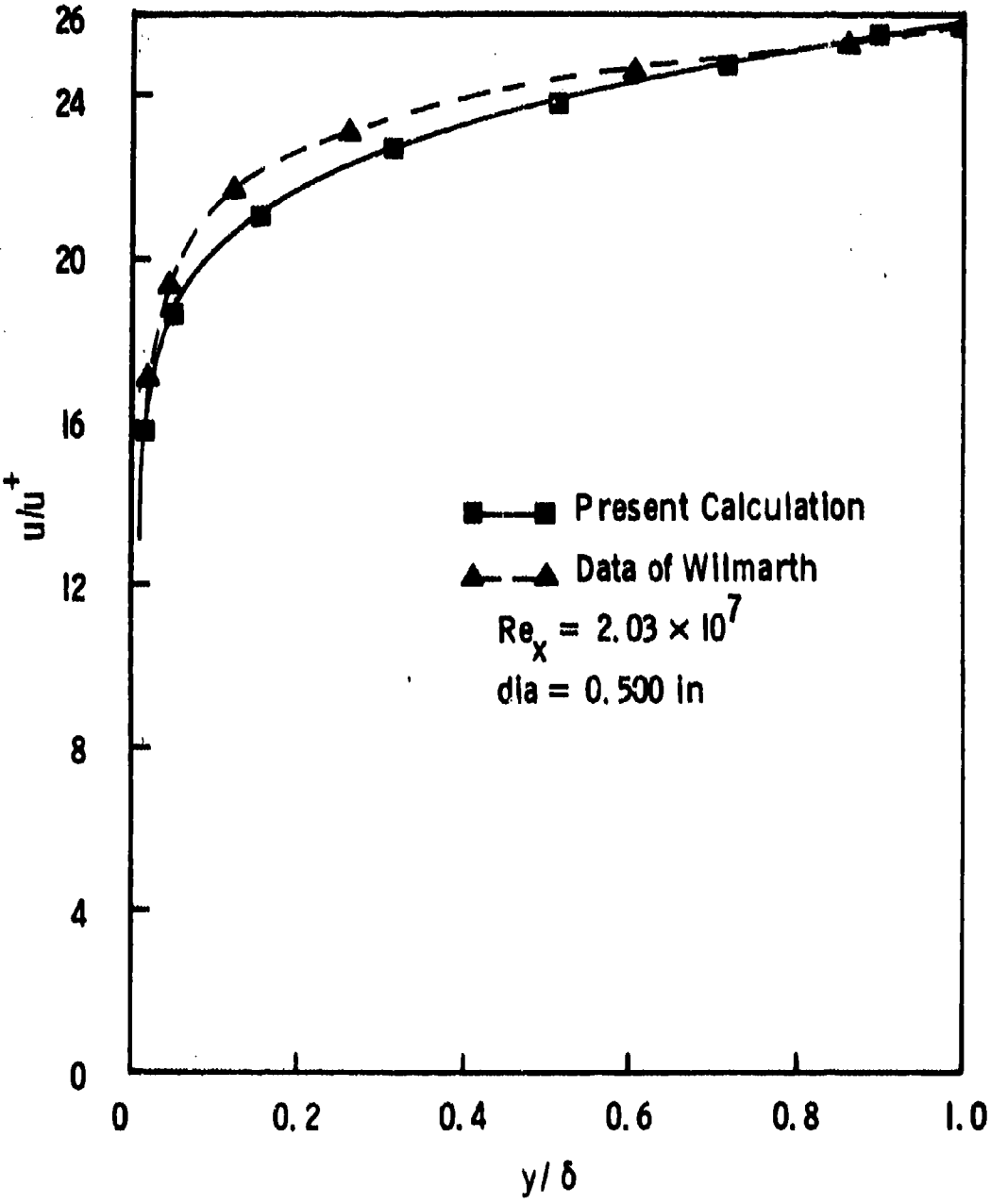

Fig. 6 Comparison of velocity profiles over case II cylinder

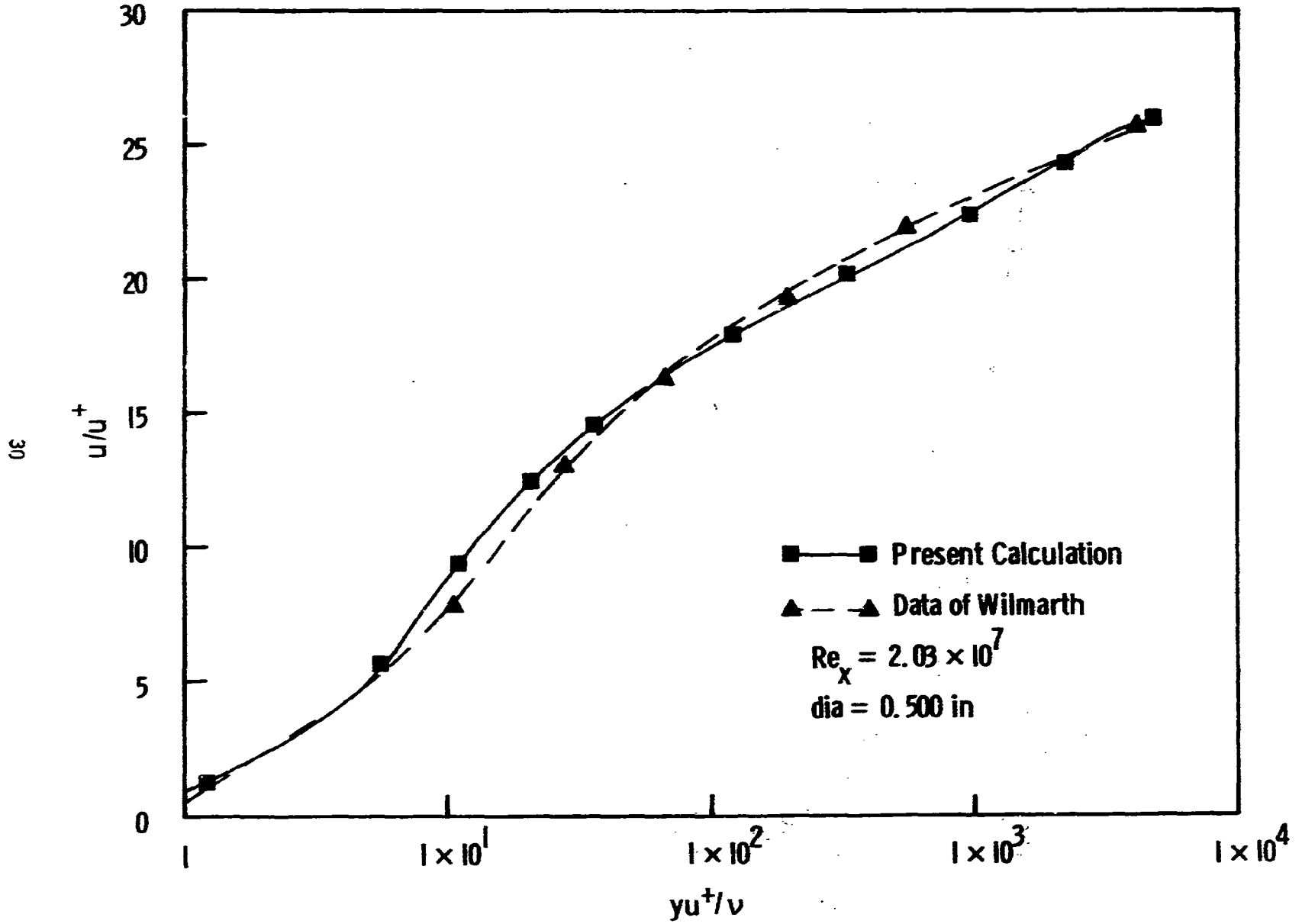

Fig. 7 Comparison of Law of the Wall velocity profiles over case II cylinder

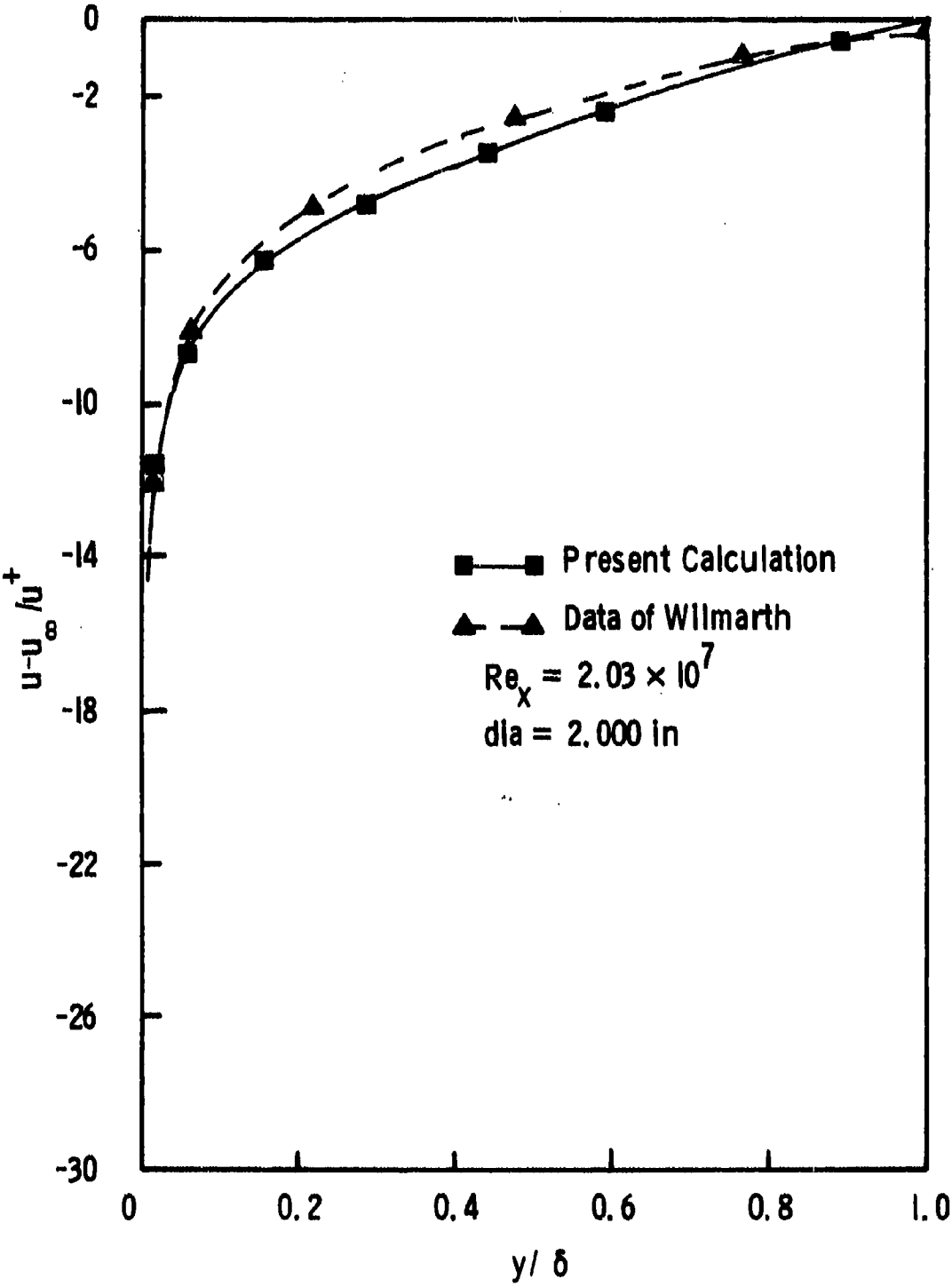

Fig. 8 Velocity defect profiles over a case 14 cylinder

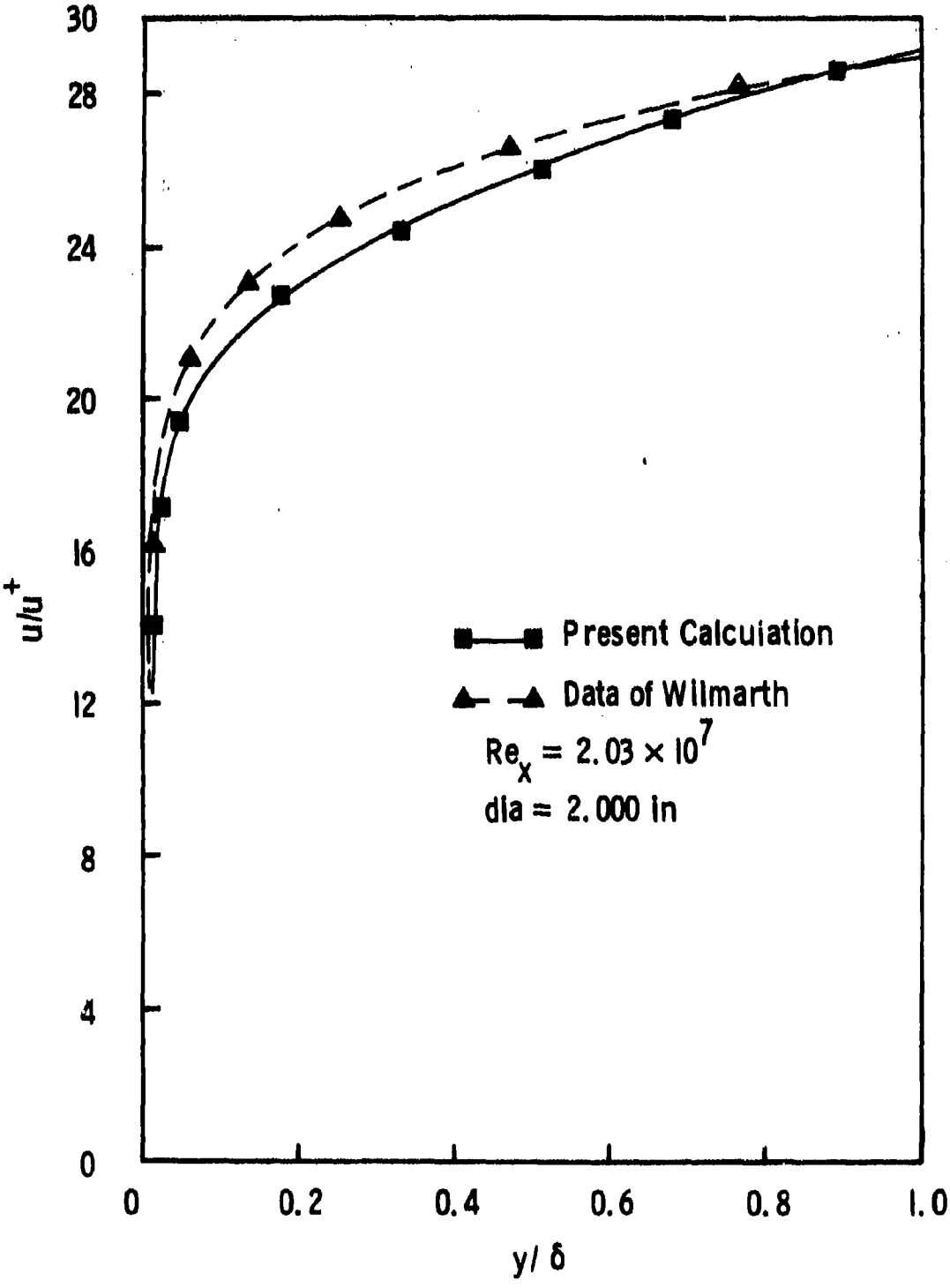

Fig. 9 Velocity profile over a case 14 cylinder

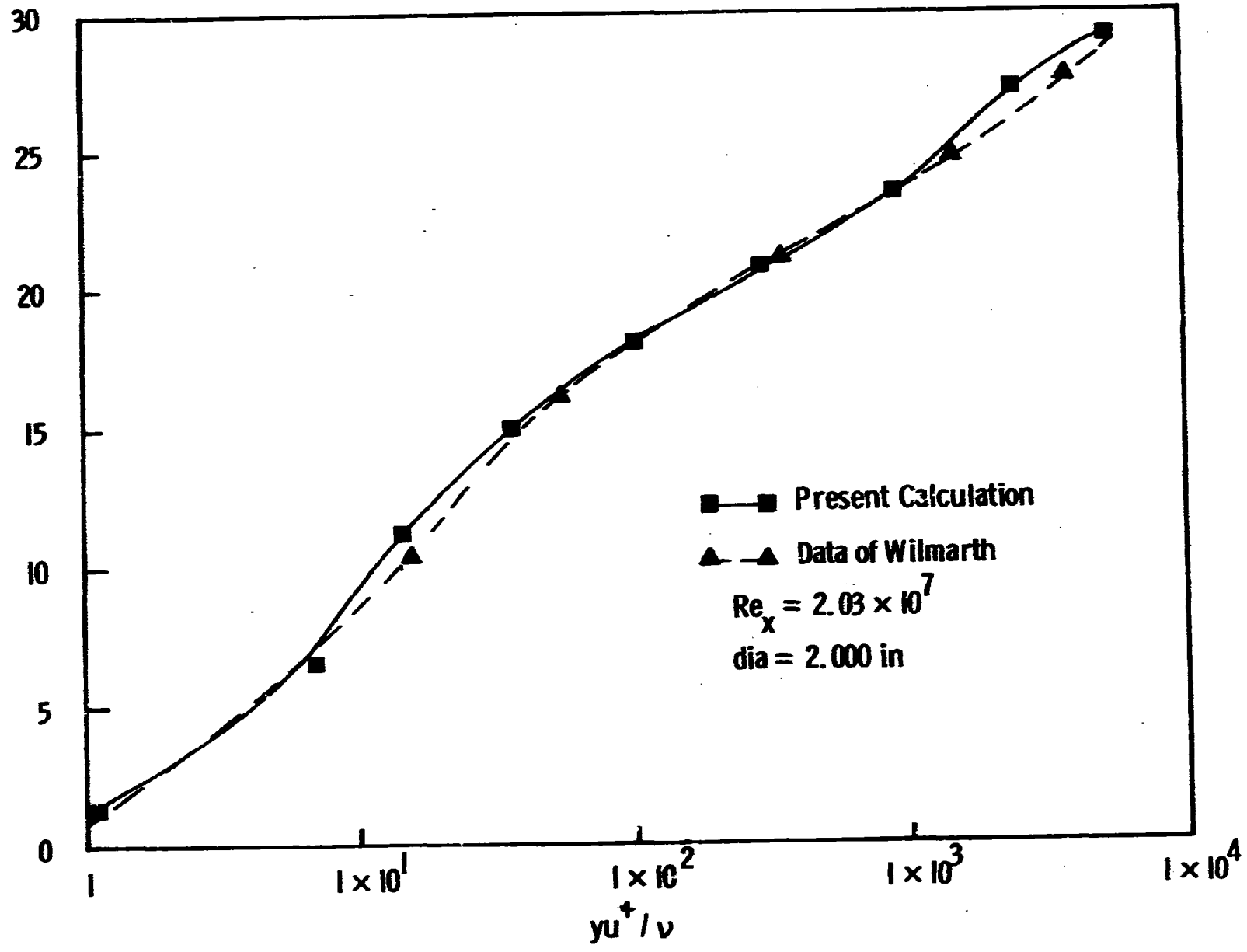

Fig. 10 Law of the Wall velocity profiles over a case 14 cylinder

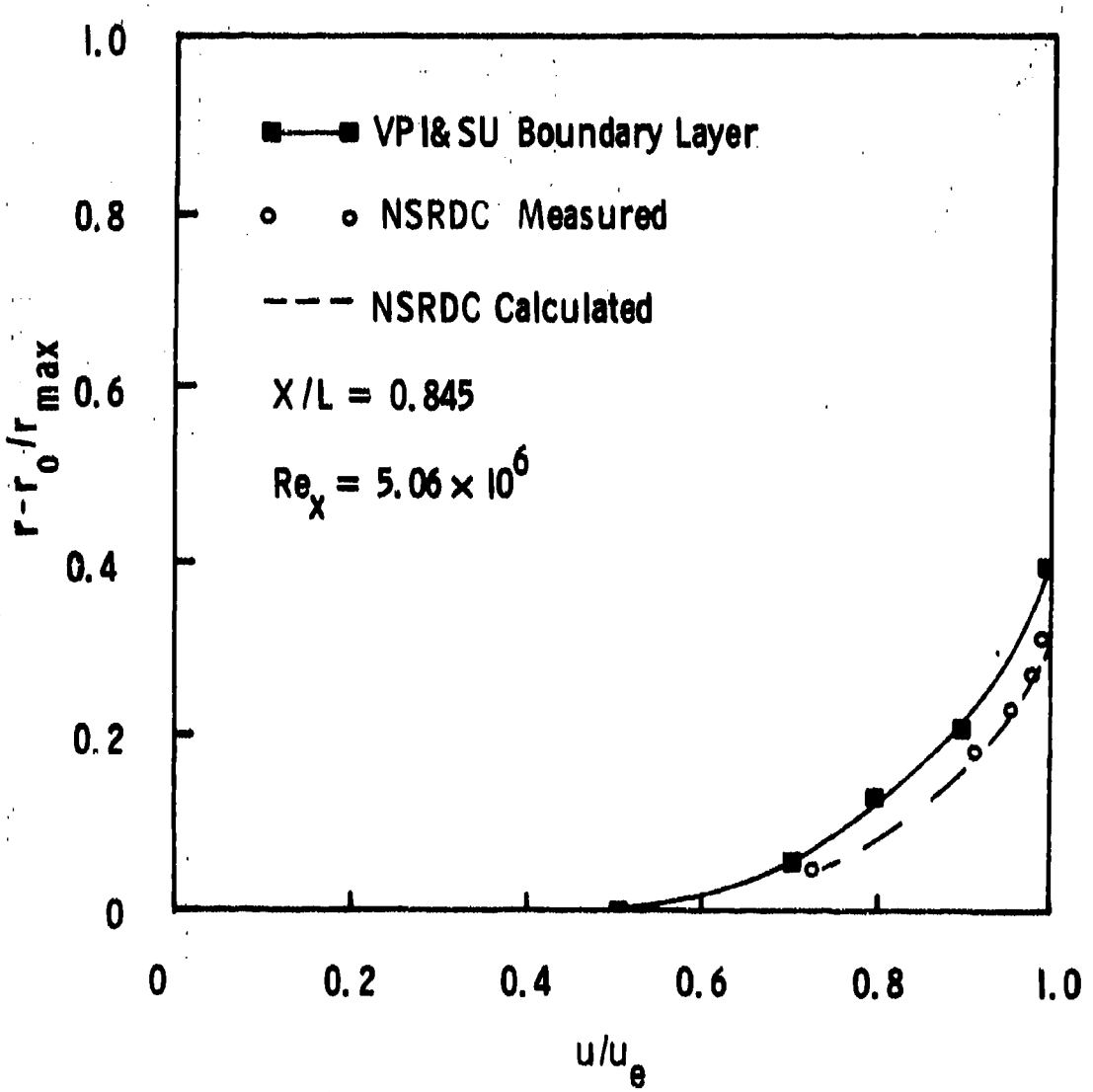

Fig. 11 Velocity profiles of test case I without a propeller in operation

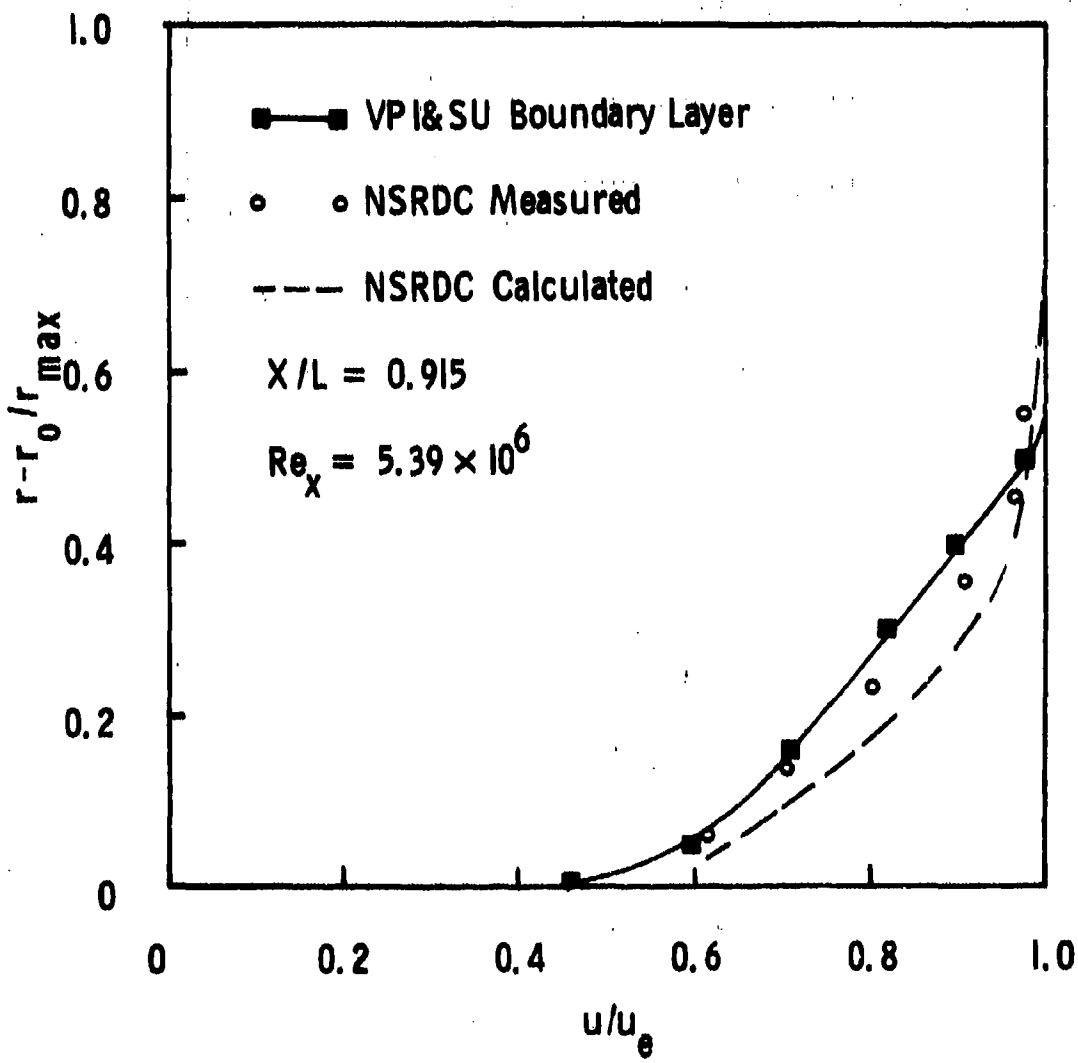

Fig. 12 Velocity profiles of test case I without a propeller in operation

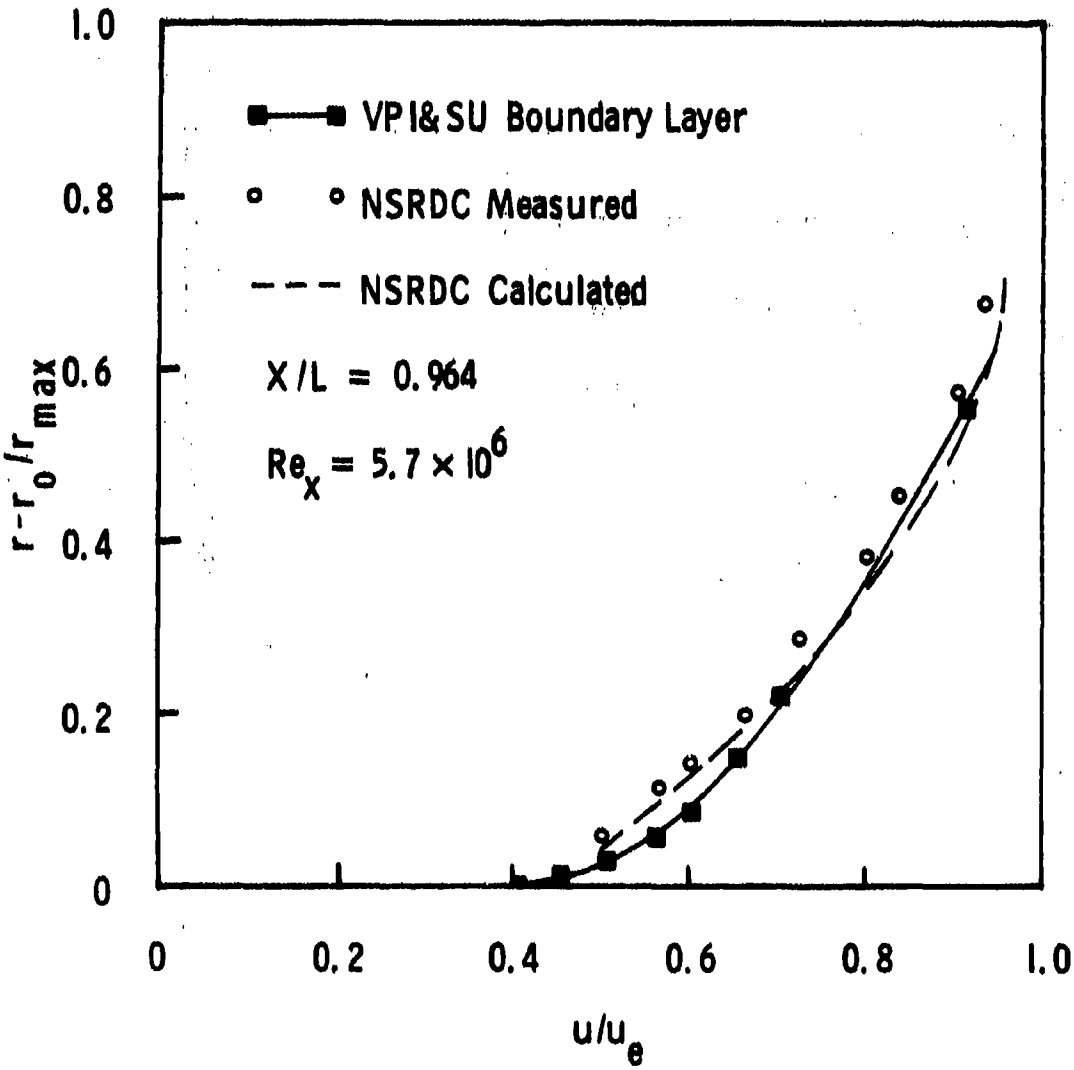

Fig. 13 Velocity profiles of test case I without a propeller in operation

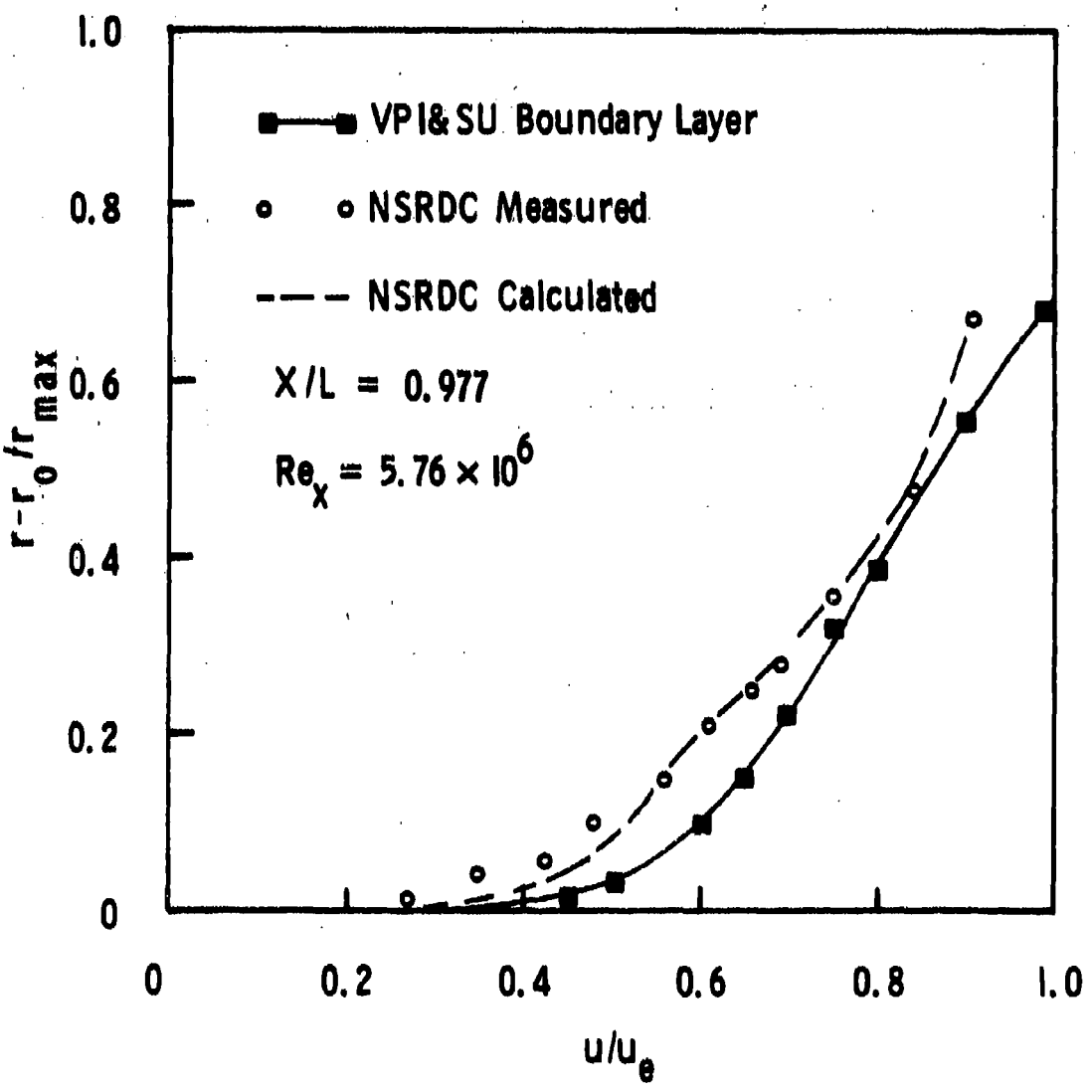

Fig. 14 Velocity profiles of test case I without a propeller in operation

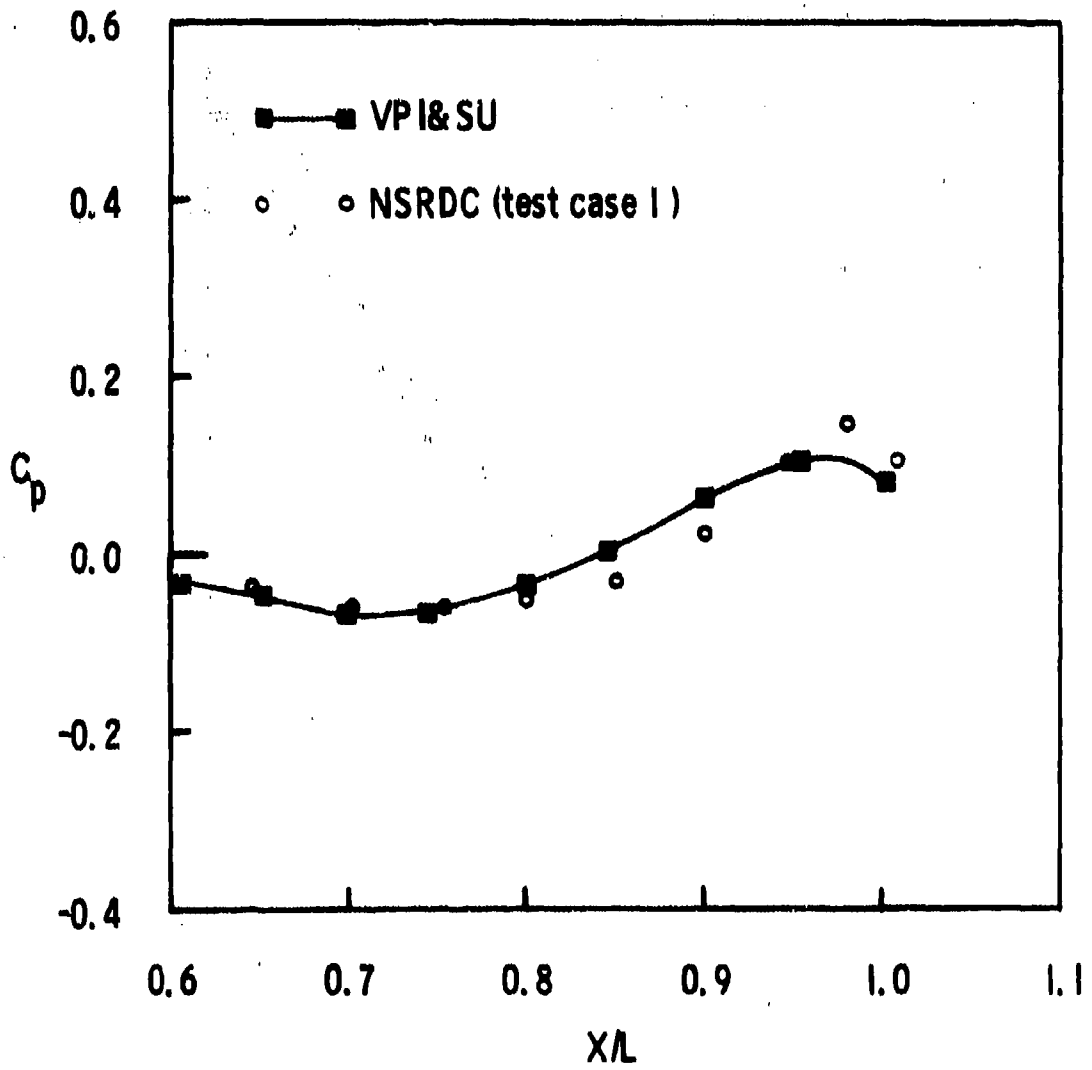

Fig. 15 Comparison of pressure distribution over submarine model ($L_A/D = 4.307$)

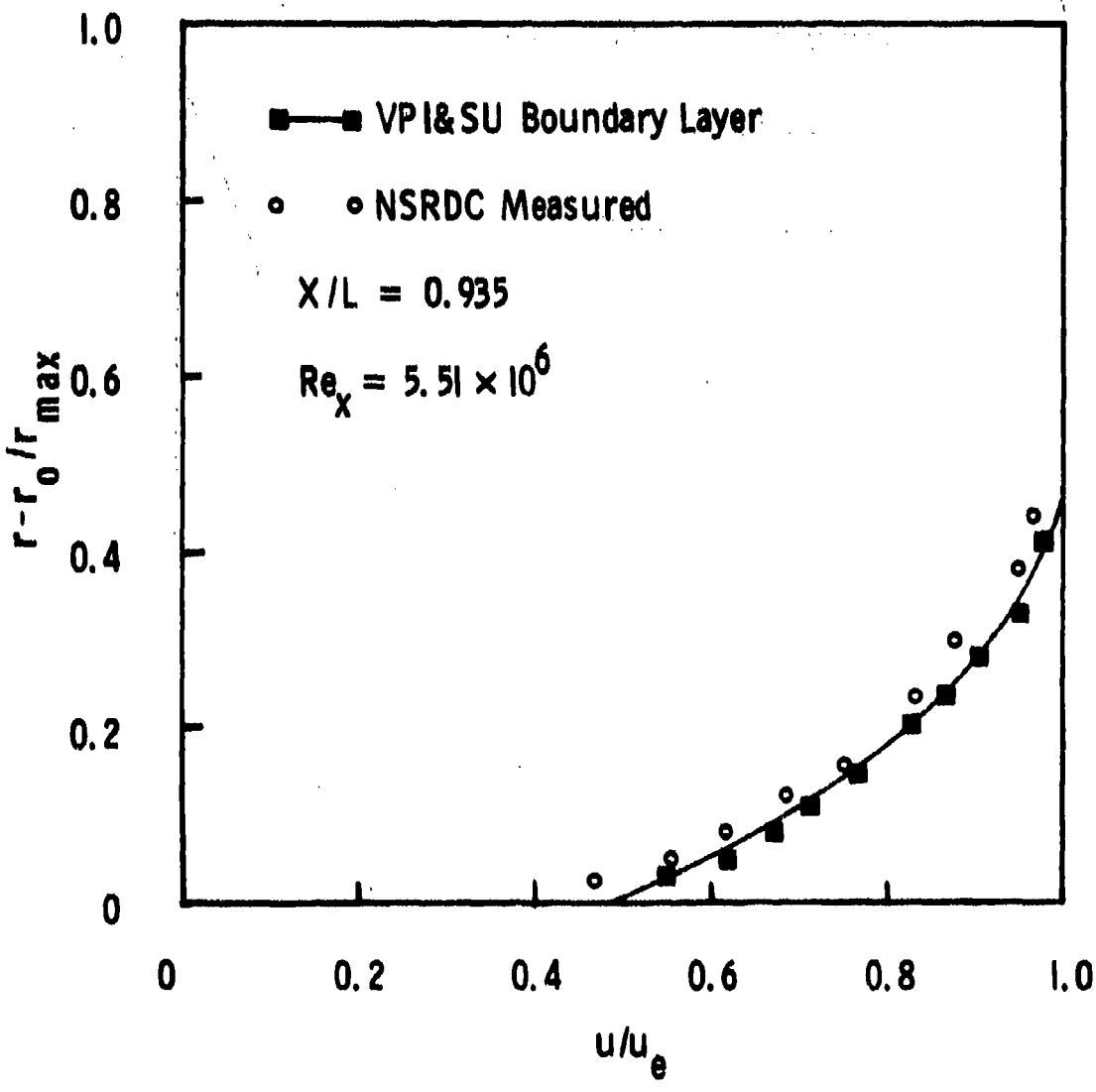

Fig. 16 Velocity profiles of test case 2 without a propeller in operation

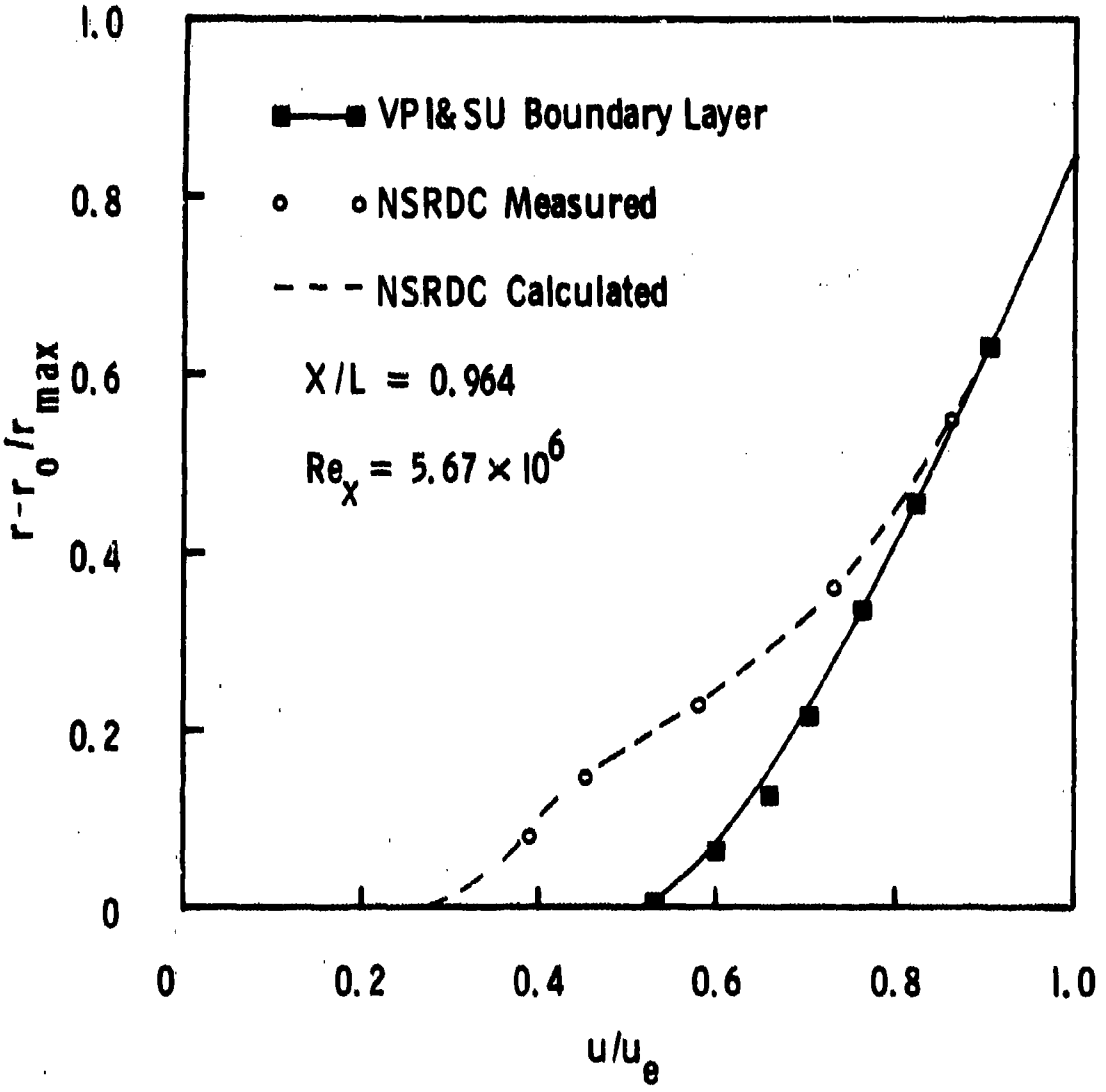

Fig. 17 Velocity profiles for test case 2 without a propeller in operation

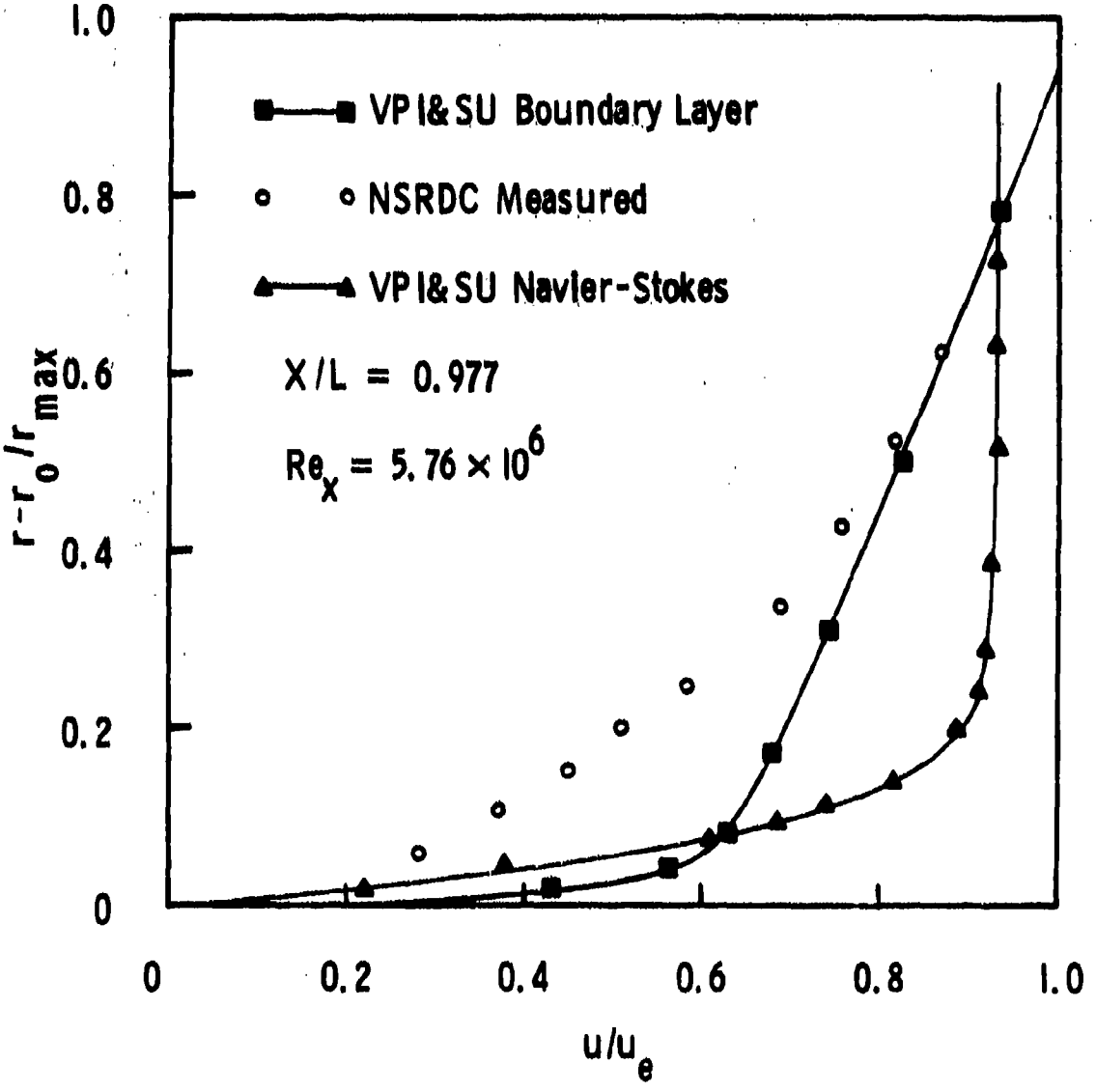

Fig. 18 Velocity profiles for test case 2 without a propeller in operation

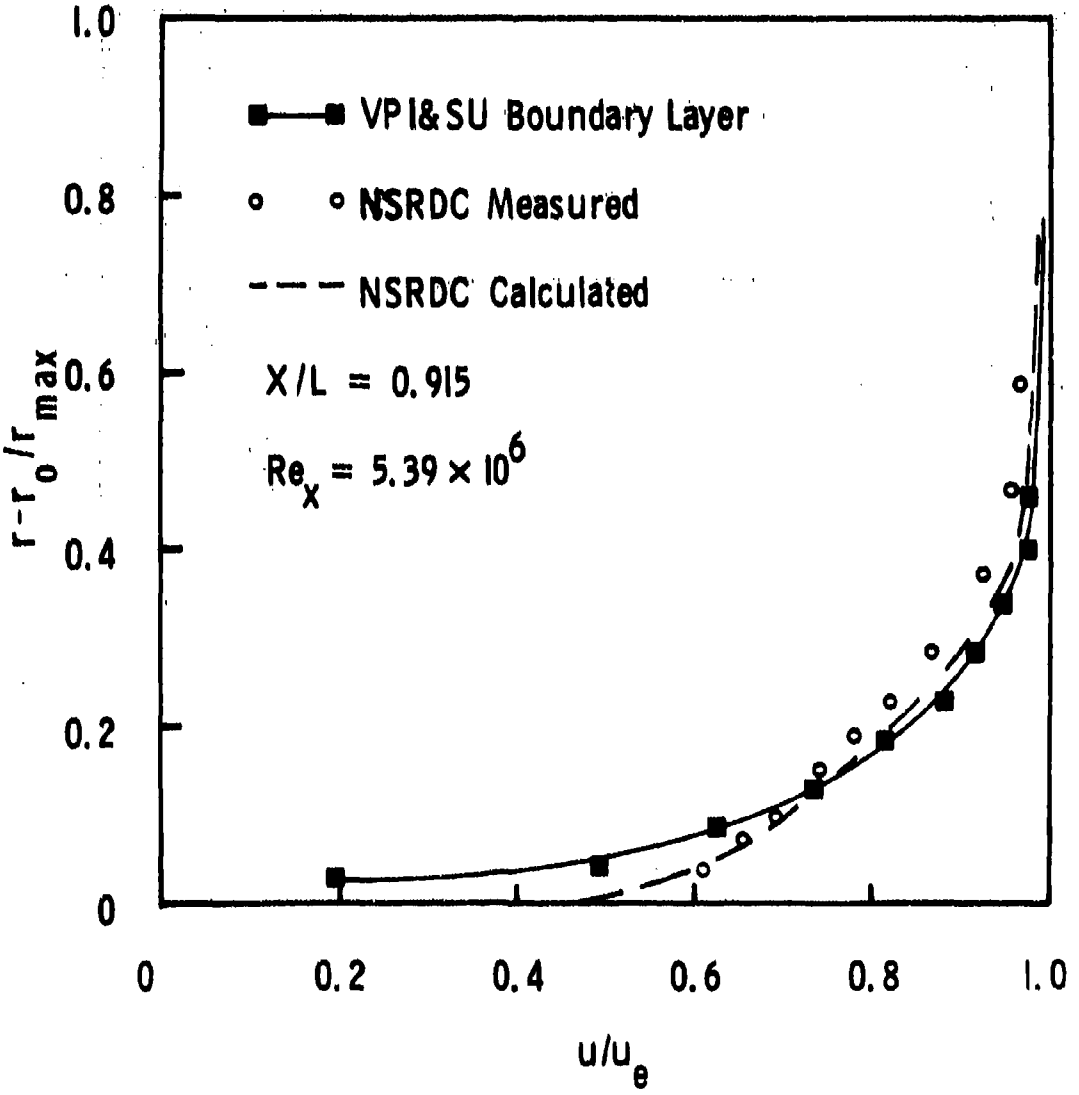

Fig. 19 Velocity profiles of test case 1 with a propeller in operation

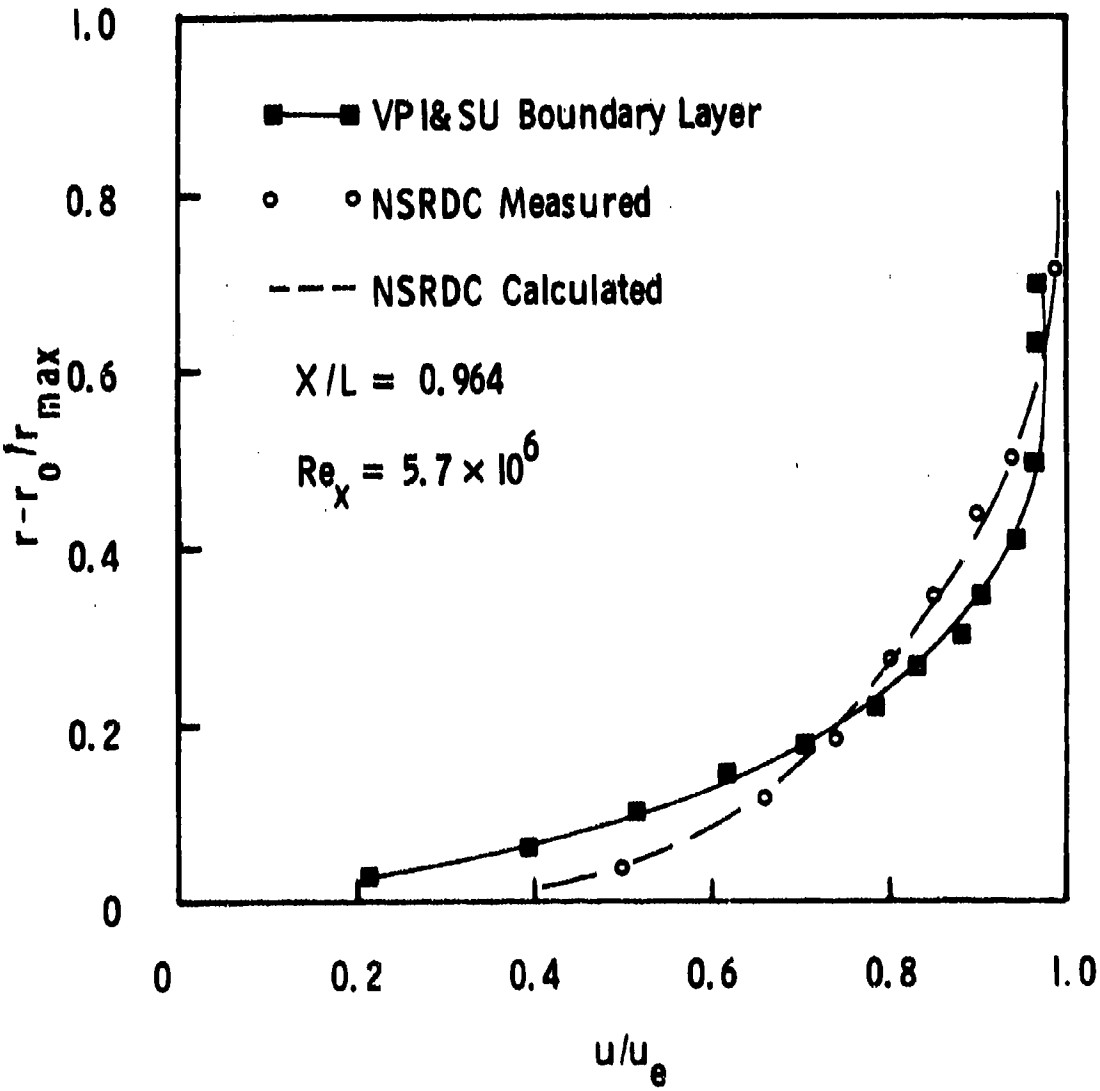

Fig. 20 Velocity profiles of test case I with a propeller in operation

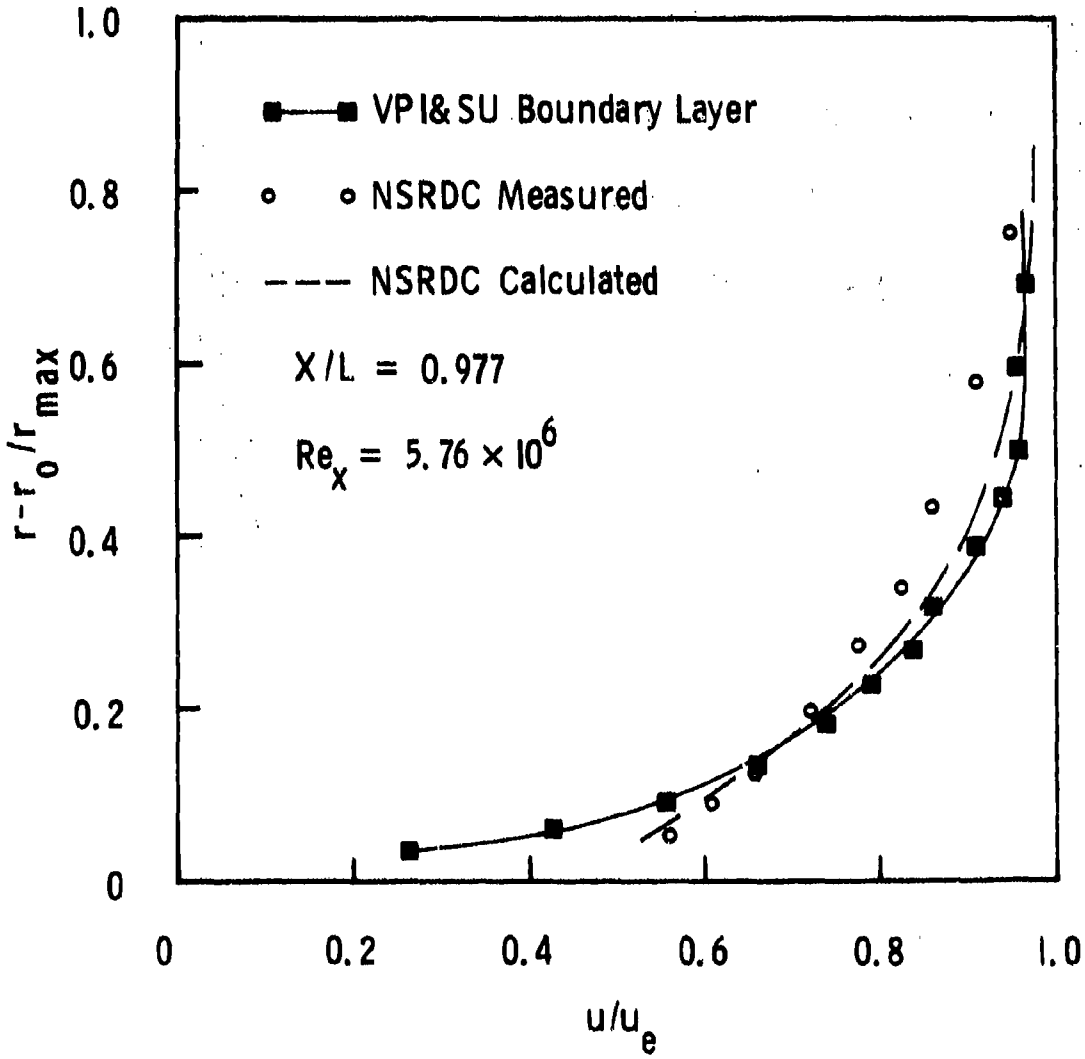

Fig. 21 Velocity profiles of test case 1 with a propeller in operation

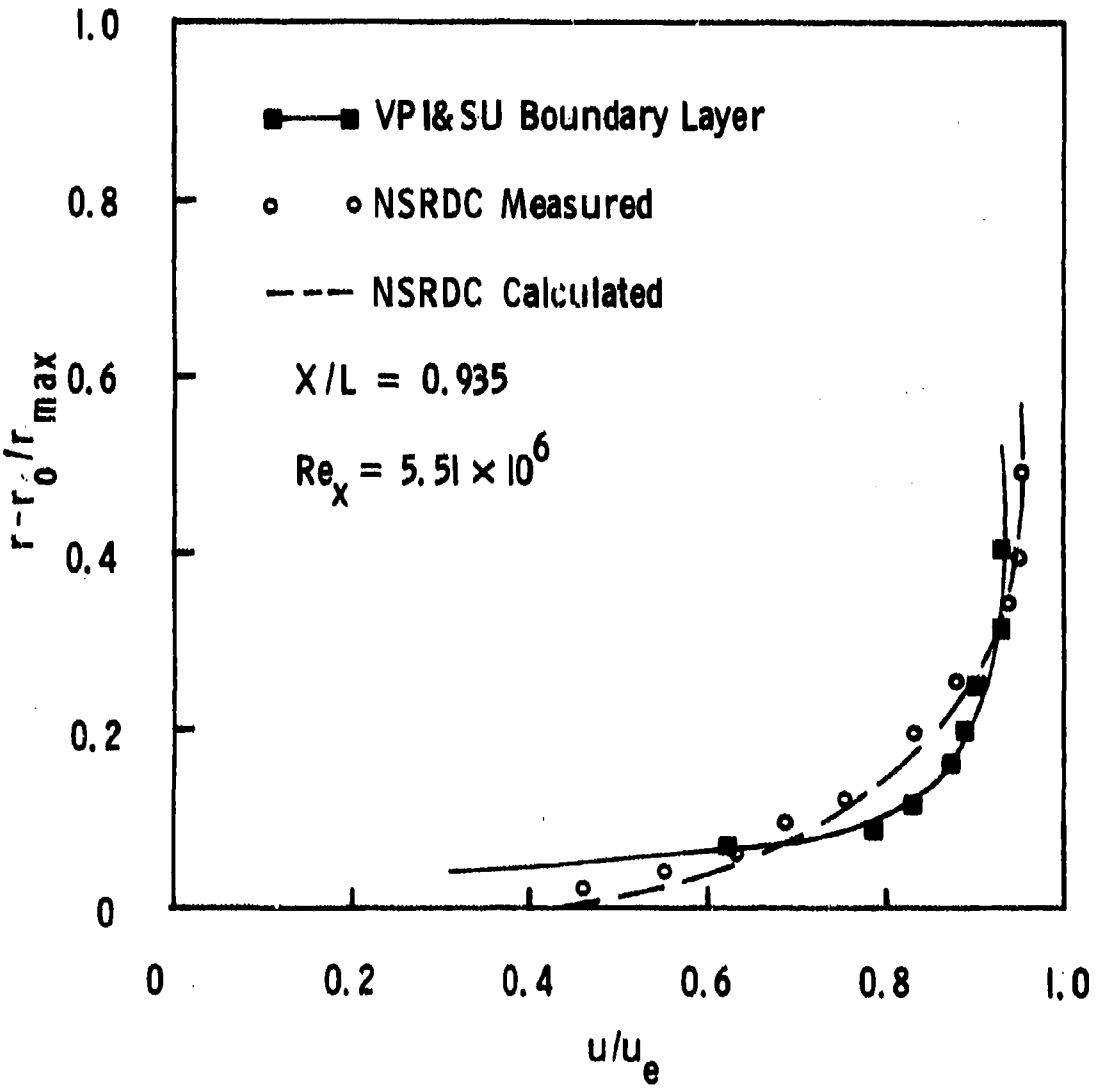

Fig. 22 Velocity profiles of test case 2 with a propeller in operation

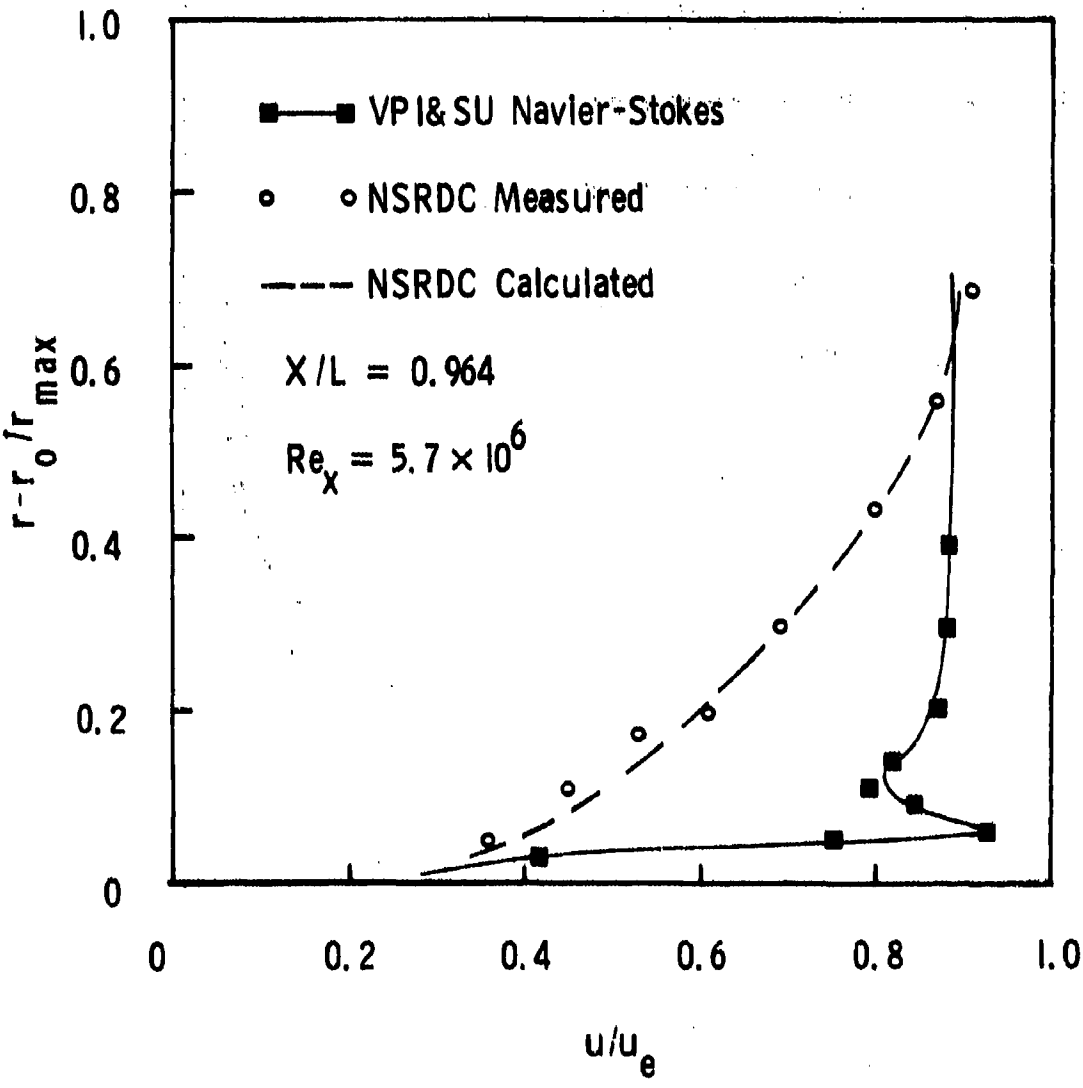

Fig. 23 Velocity profiles of test case 2 with a propeller in operation

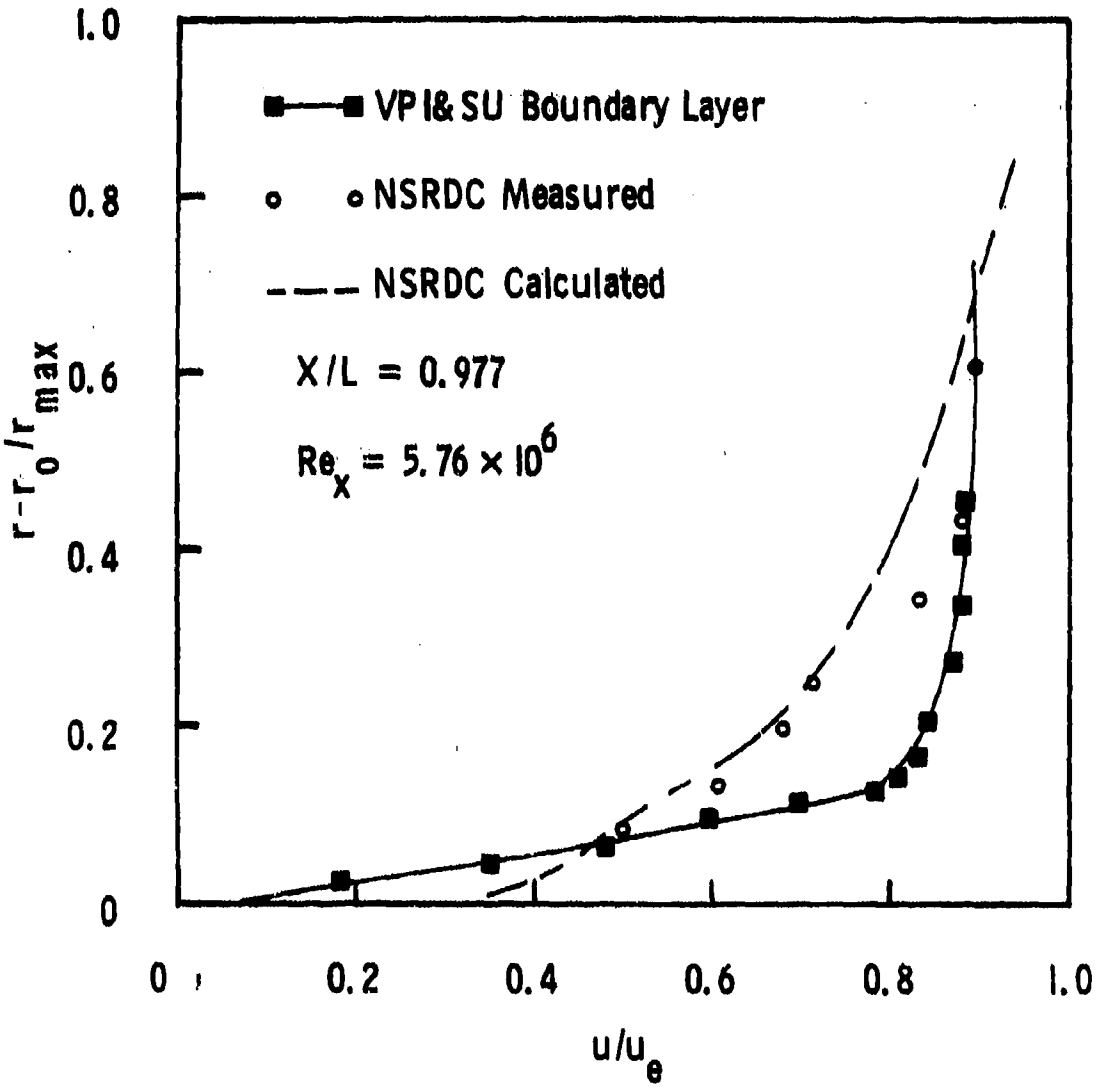

Fig. 24 Velocity profiles of test case 2 with a propeller in operation

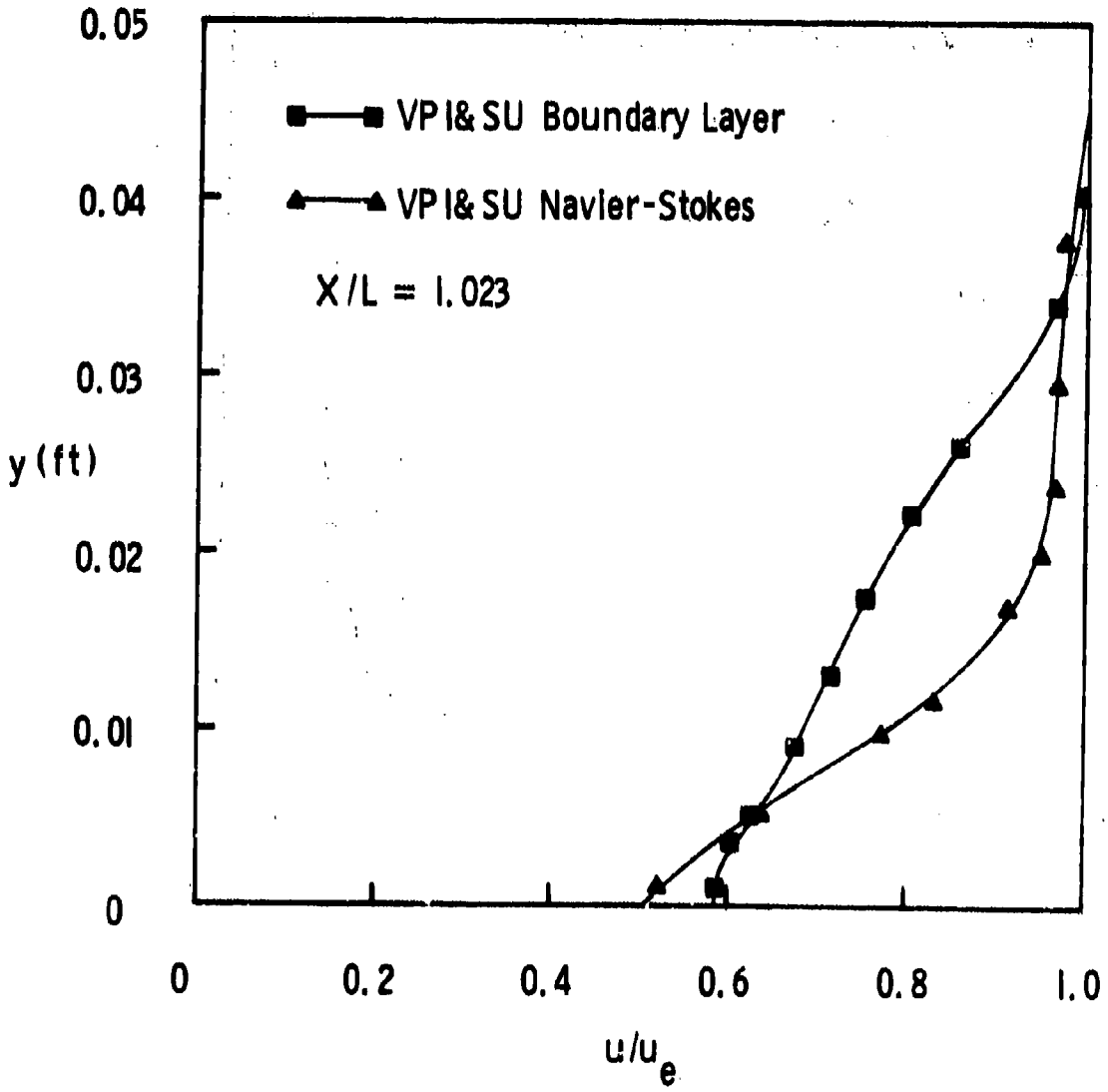

Fig. 25 Velocity profiles in the near wake (X/L = 1.023) of test case 1 without a propeller in operation

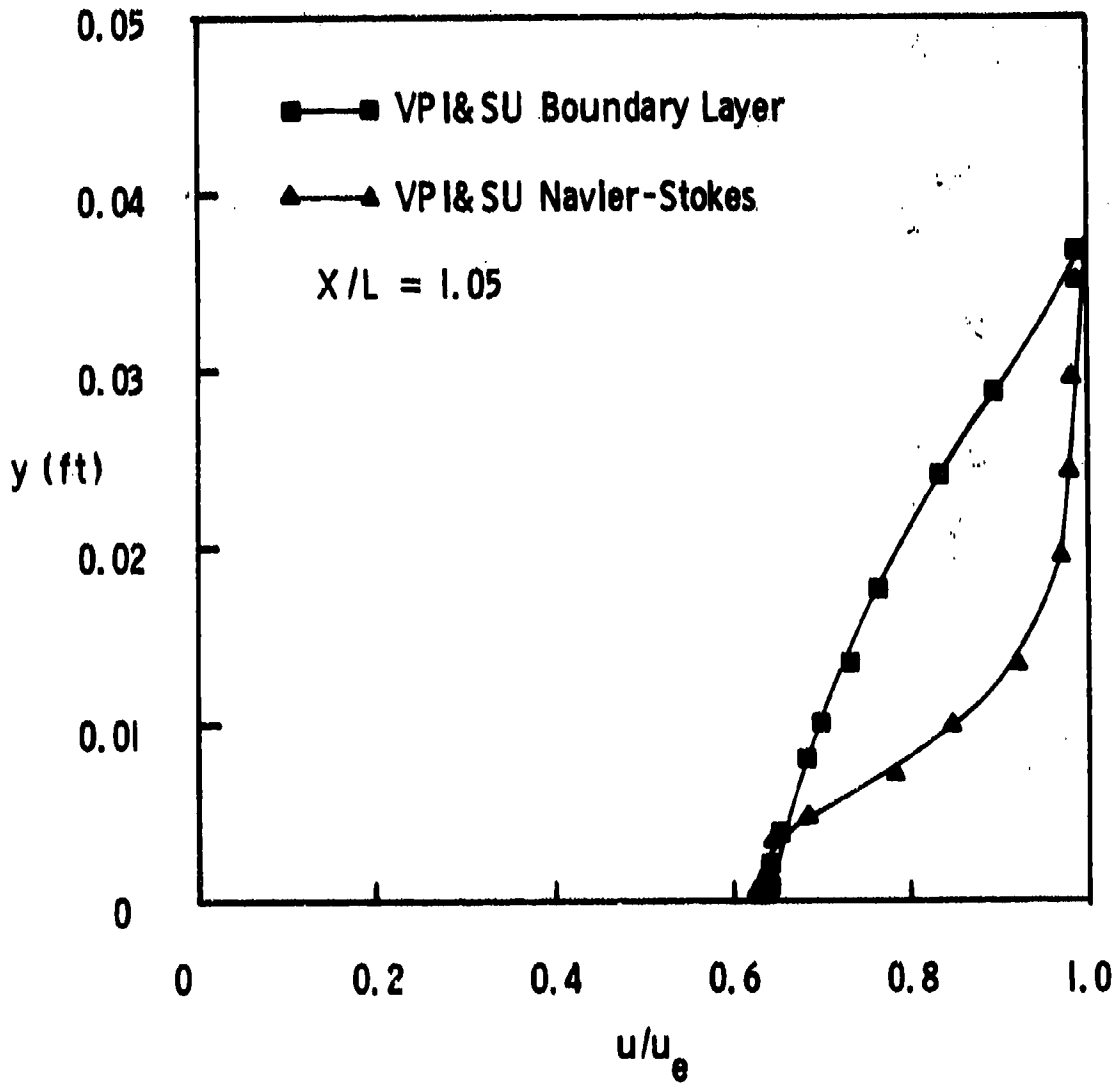

Fig. 26 Velocity profiles in the near wake (X/L = 1.05) of test case 1 without a propeller in operation

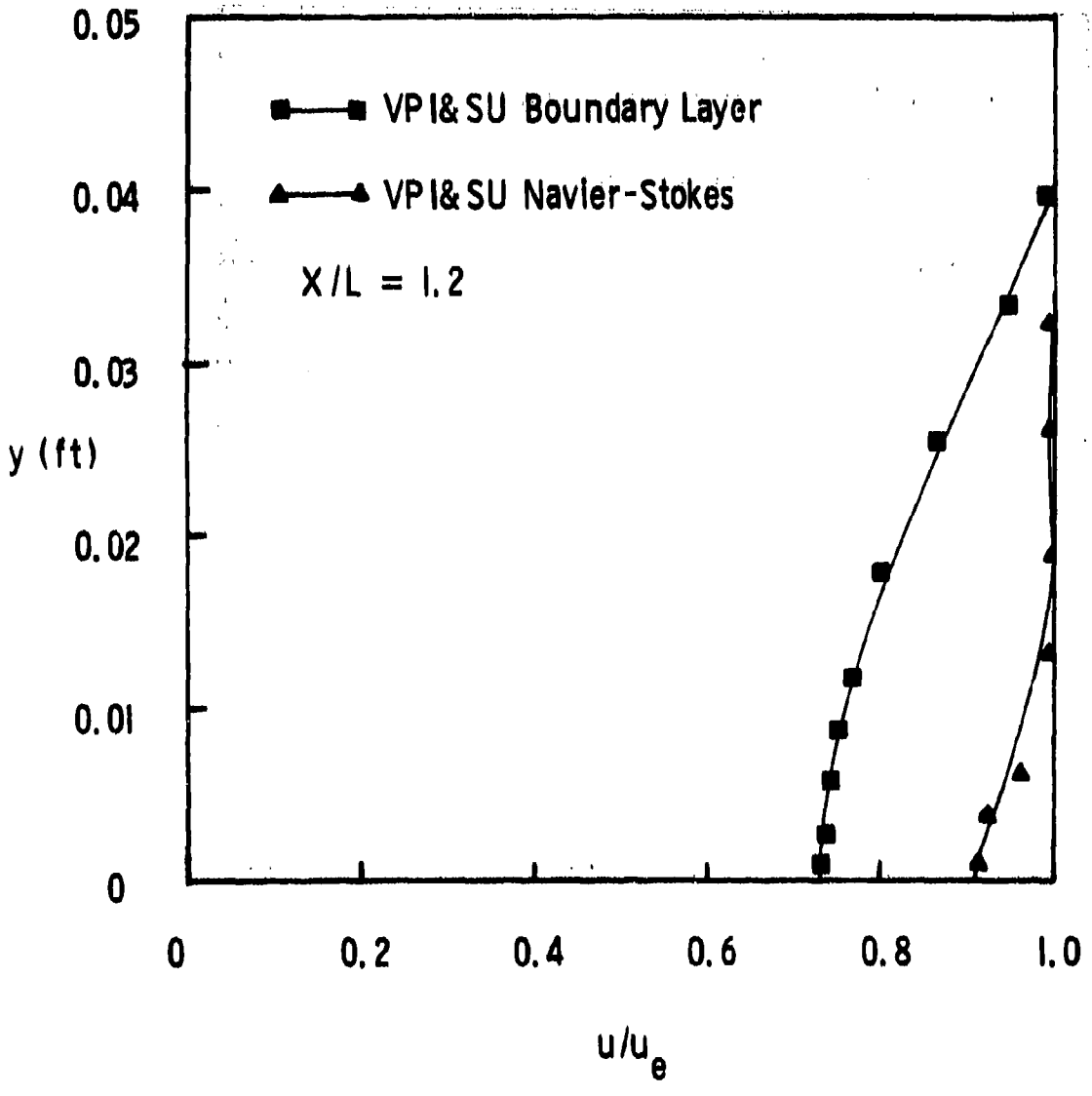

Fig. 27 Velocity profiles in the near wake (X/L = 1.2) of test case 1 without a propeller in operation

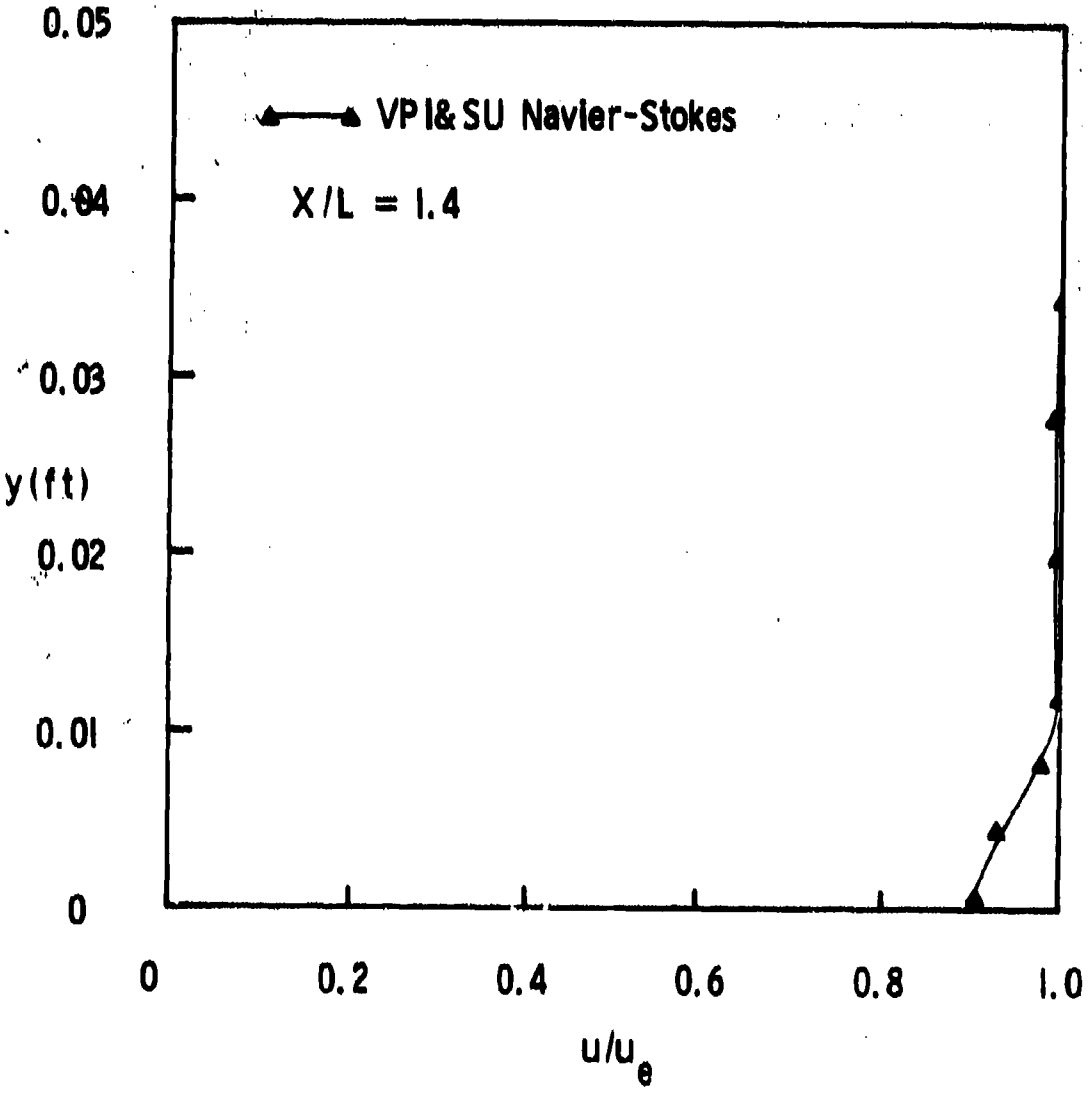

Fig. 28 Velocity profiles in the near wake (X/L = 1.4) of test case 1 without a propeller in operation

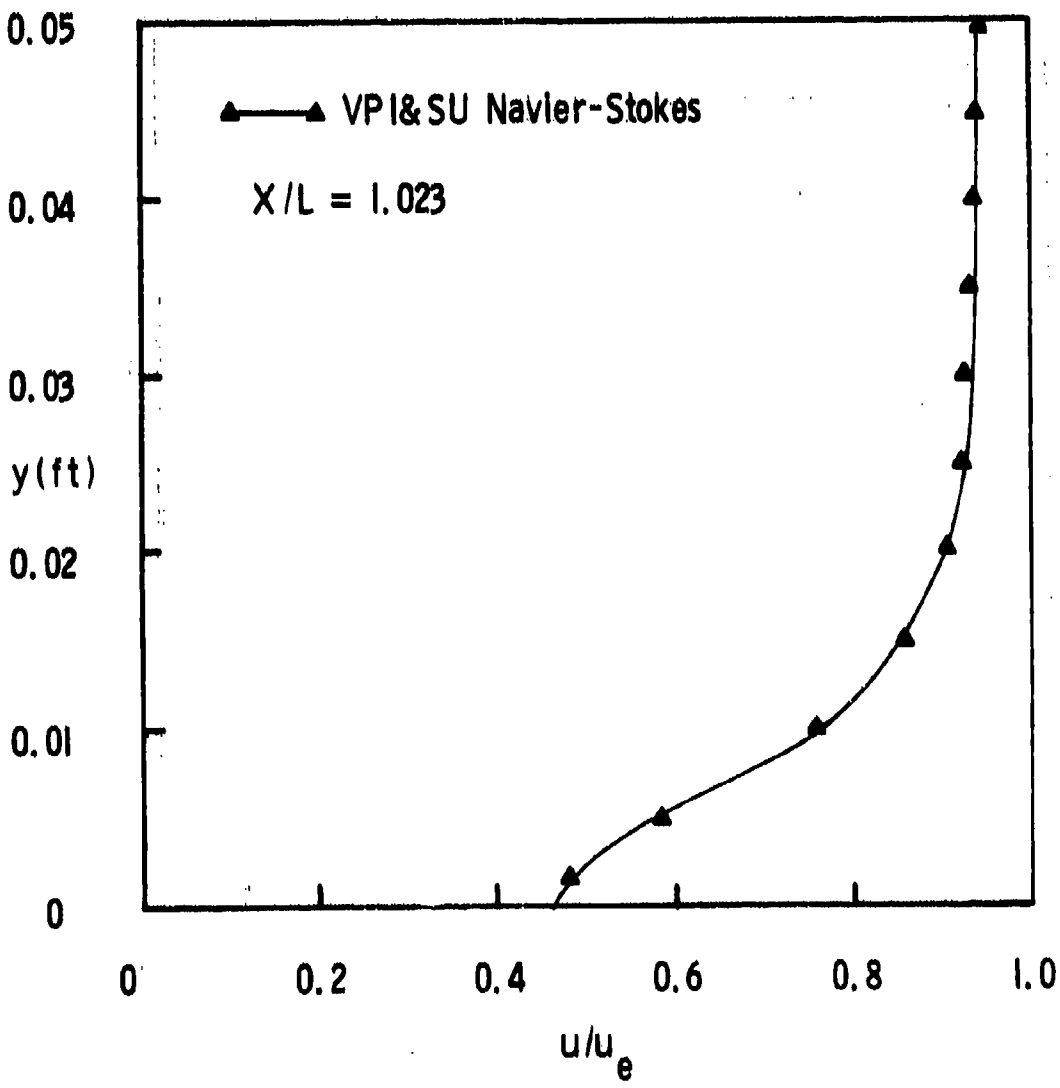

Fig. 29 Velocity profiles in the near wake (X/L = 1.023) of test case 1 with a propeller in operation

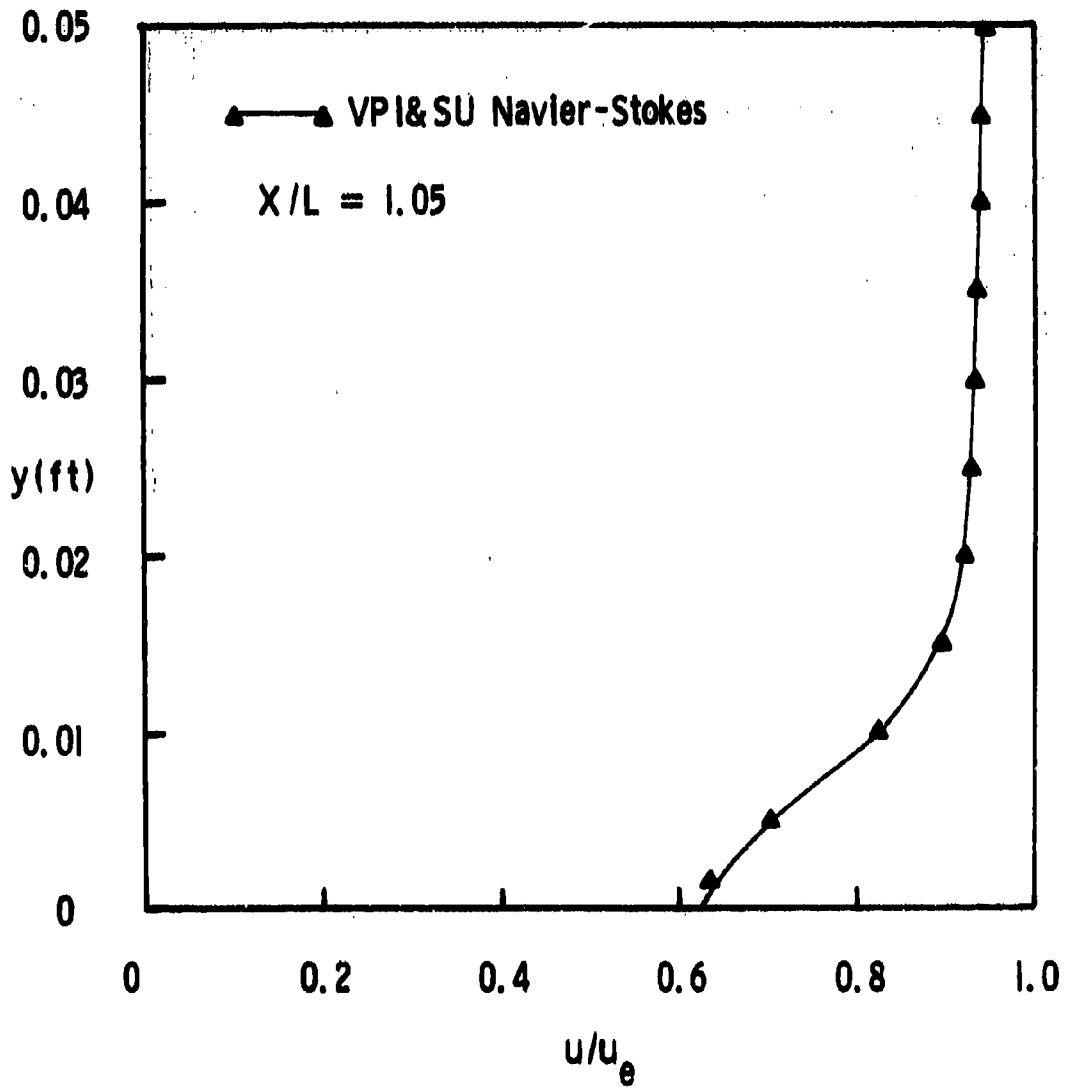

Fig. 30 Velocity profiles in the near wake (X/L = 1.05) of test case 1 with a propeller in operation

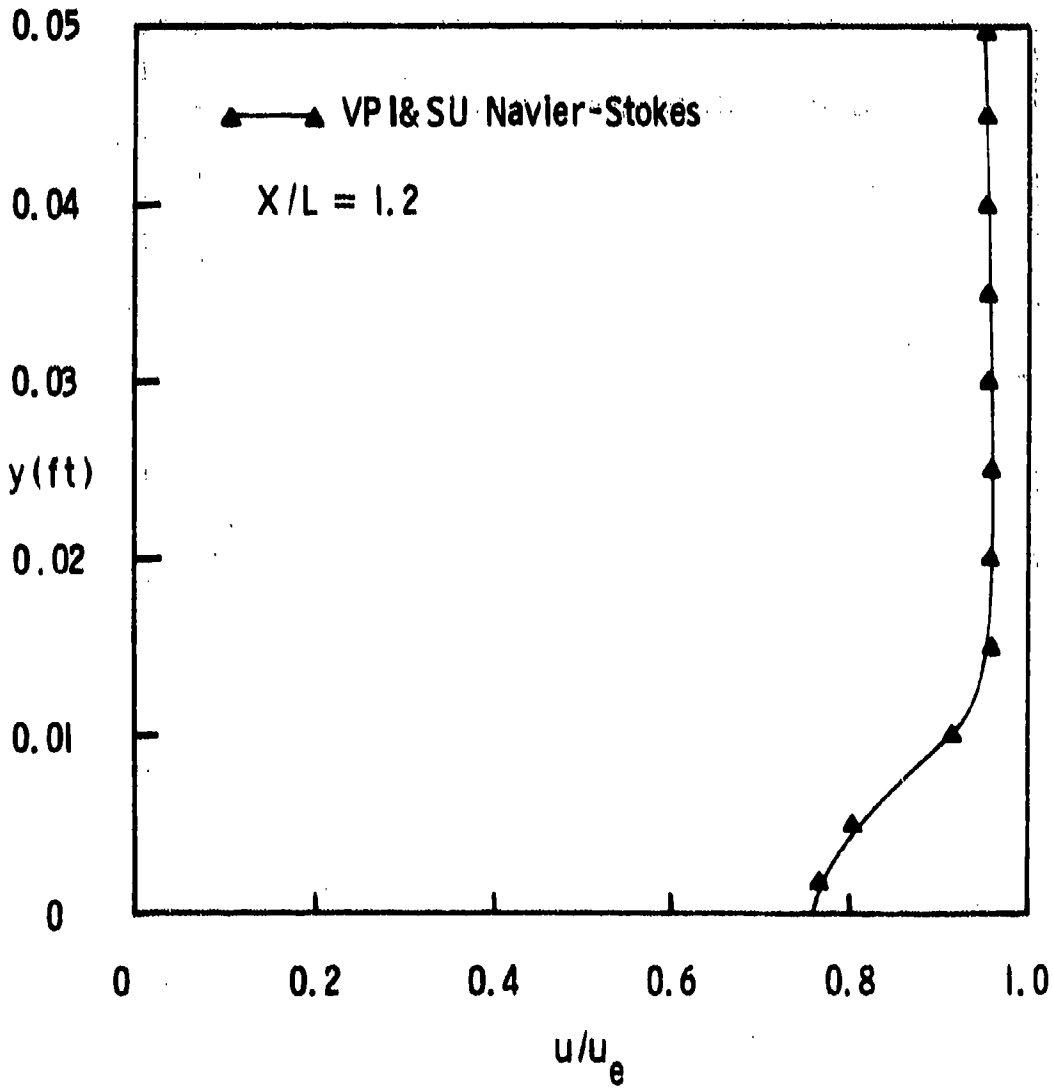

Fig. 31 Velocity profiles in the near wake (X/L = 1.2) of test case 1 with a propeller in operation

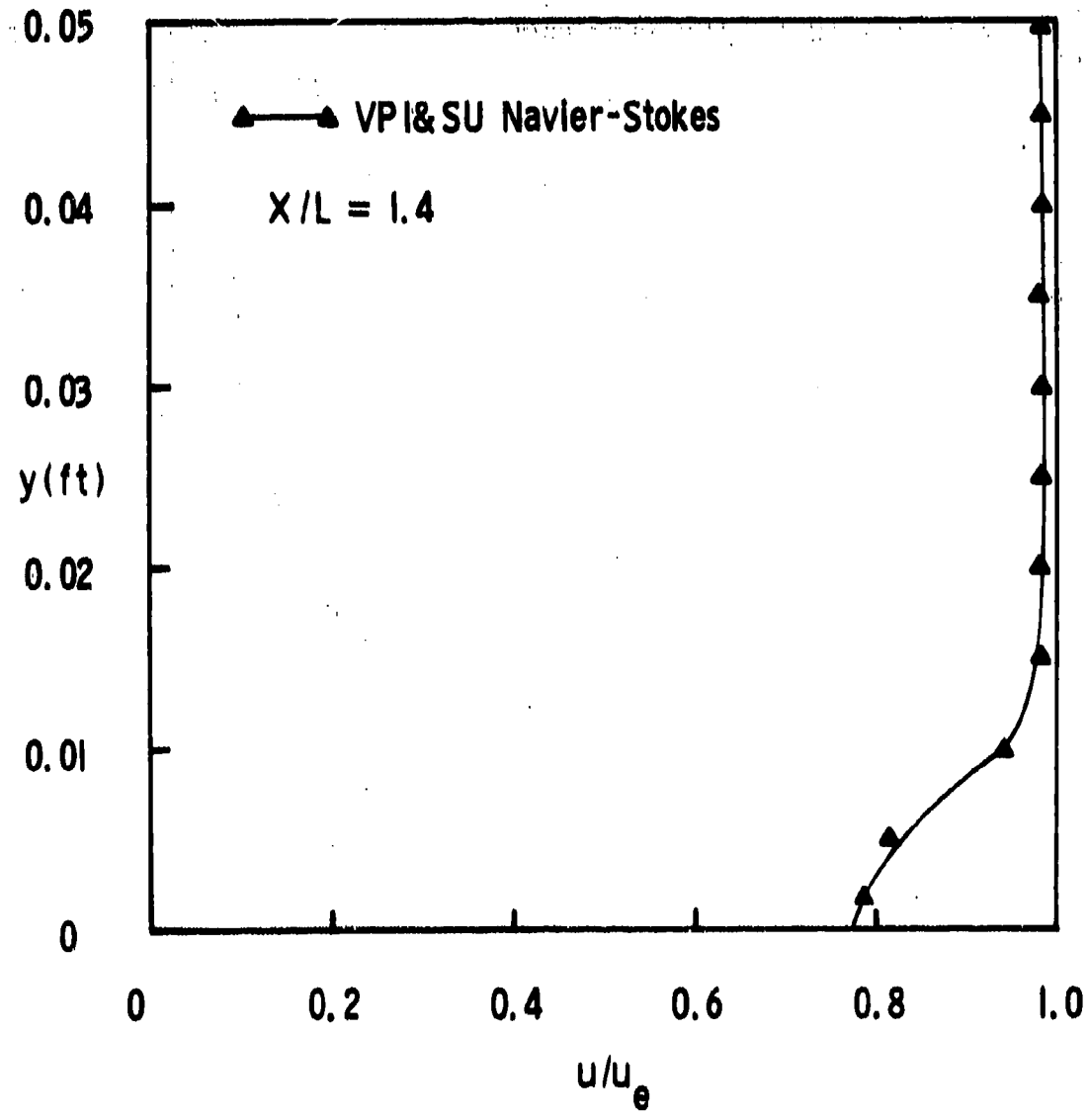

Fig. 32 Velocity profiles in the near wake (X/L = 1.4) of test case 1 with a propeller in operation

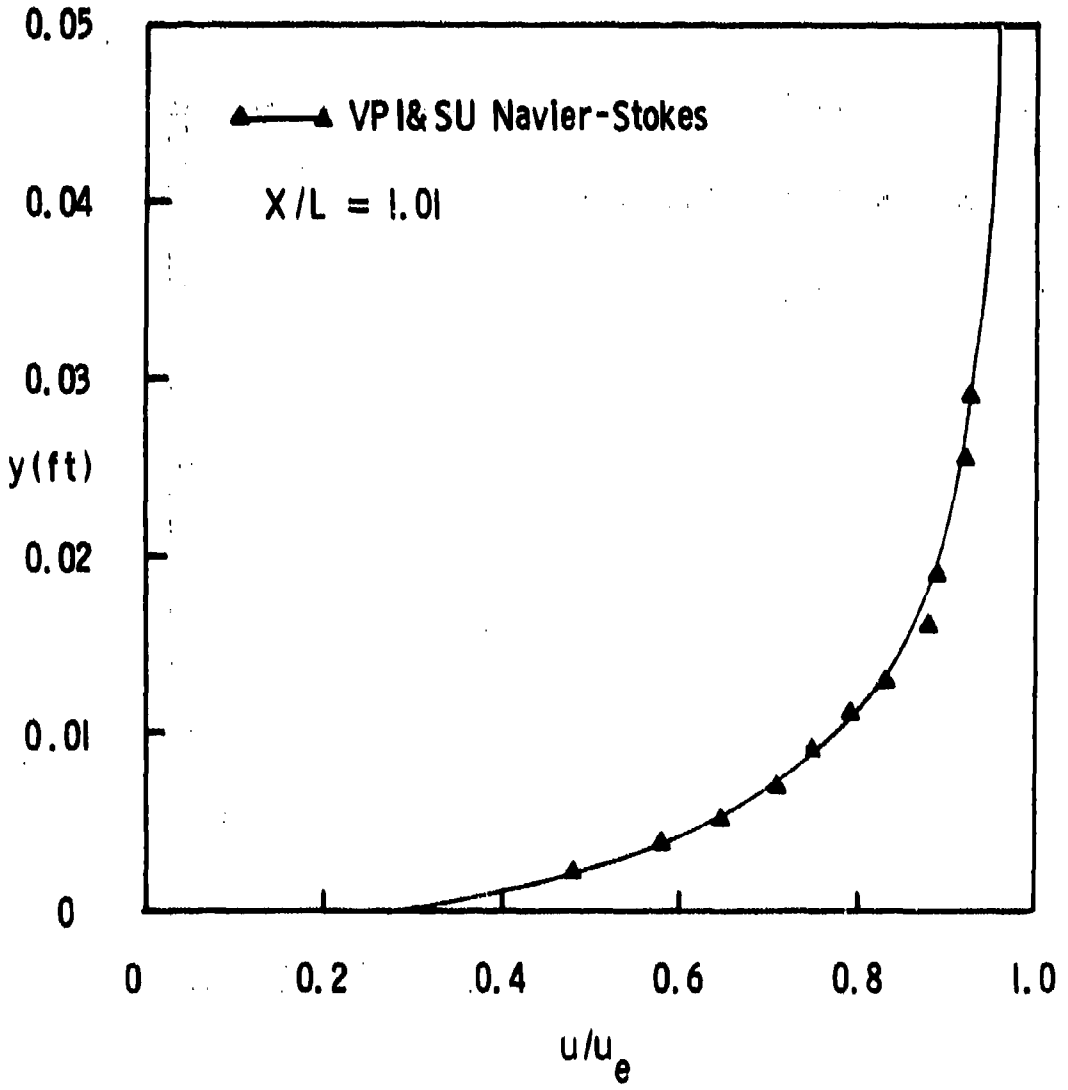

Fig. 33 Velocity profiles in the near wake (X/L = 1.0128) of test case 2 without a propeller in operation

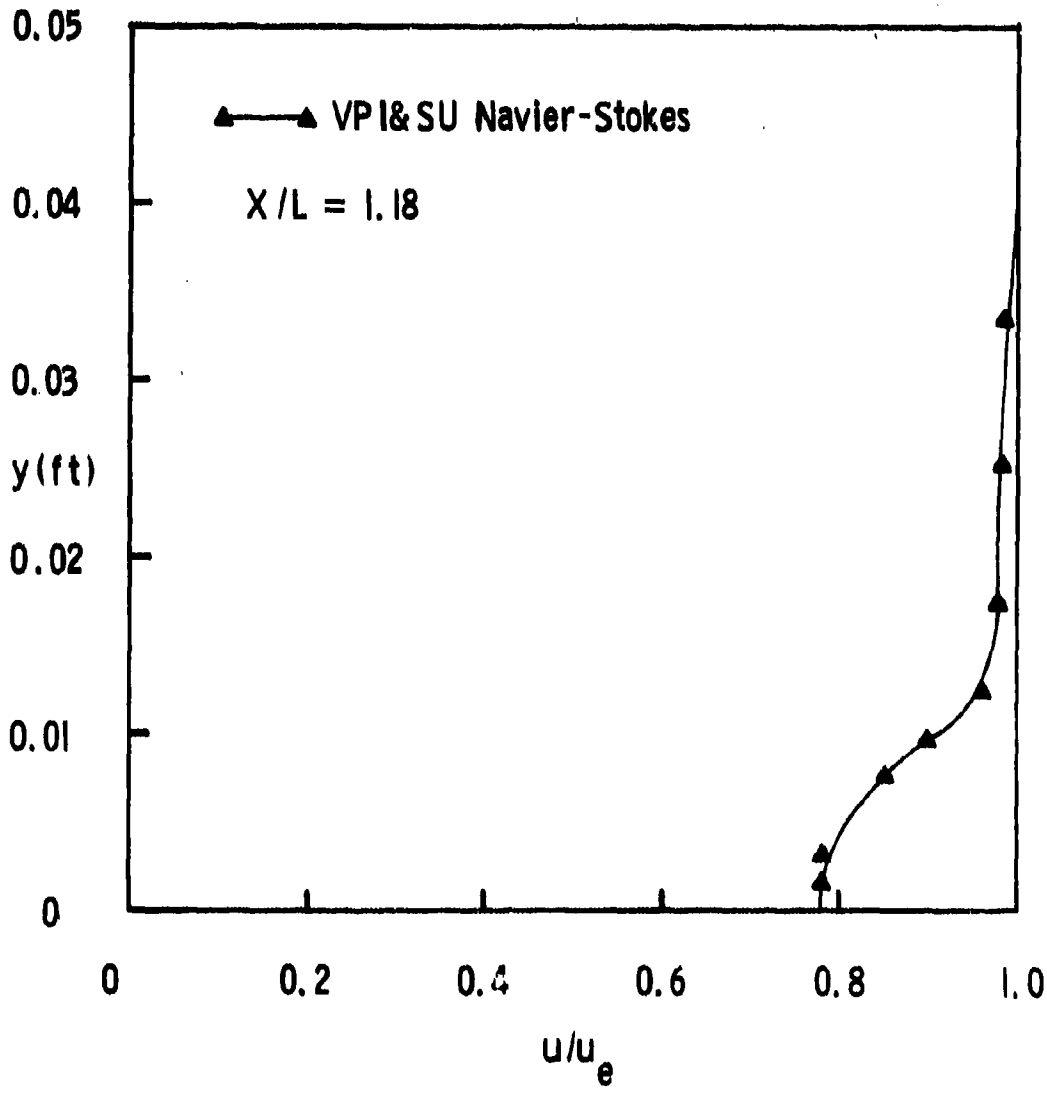

Fig. 34 Velocity profiles in the near wake (X/L = 1.18) of test case 2 without a propeller in operation

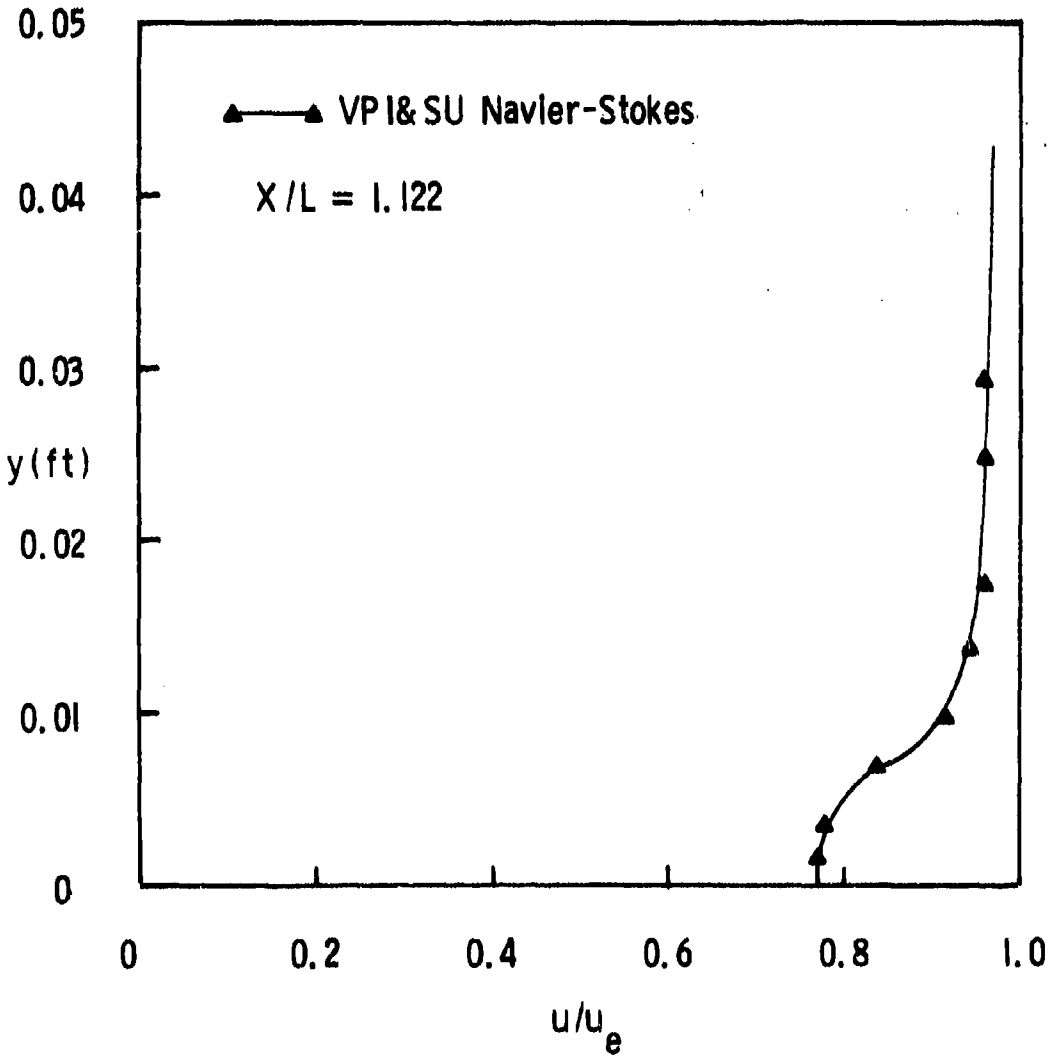

Fig. 35 Velocity profiles in the near wake (X/L = 1.122) of test case 2 without a propeller in operation

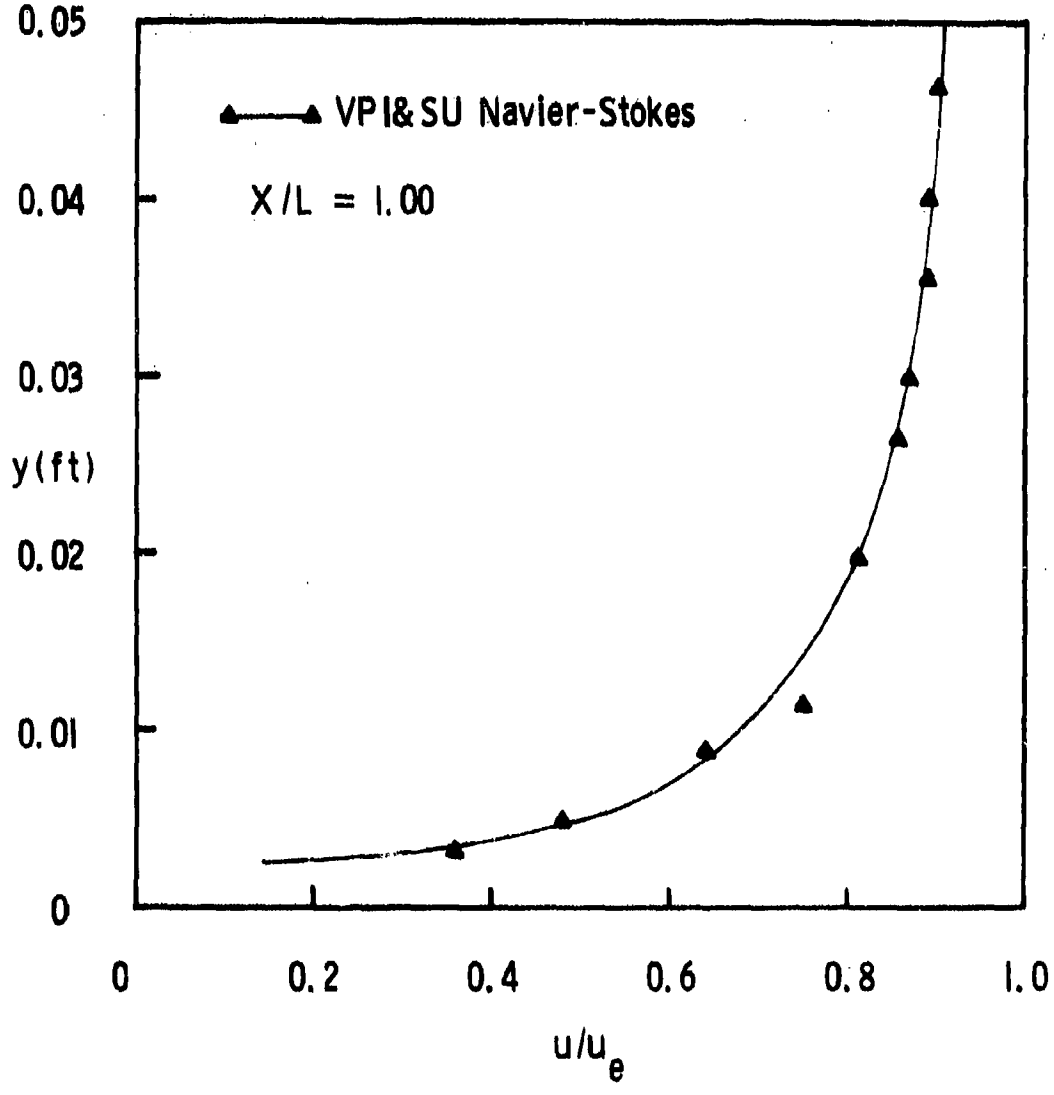

Fig. 36 Velocity profiles in the near wake (X/L = 1.00) of test case 2 with a propeller in operation

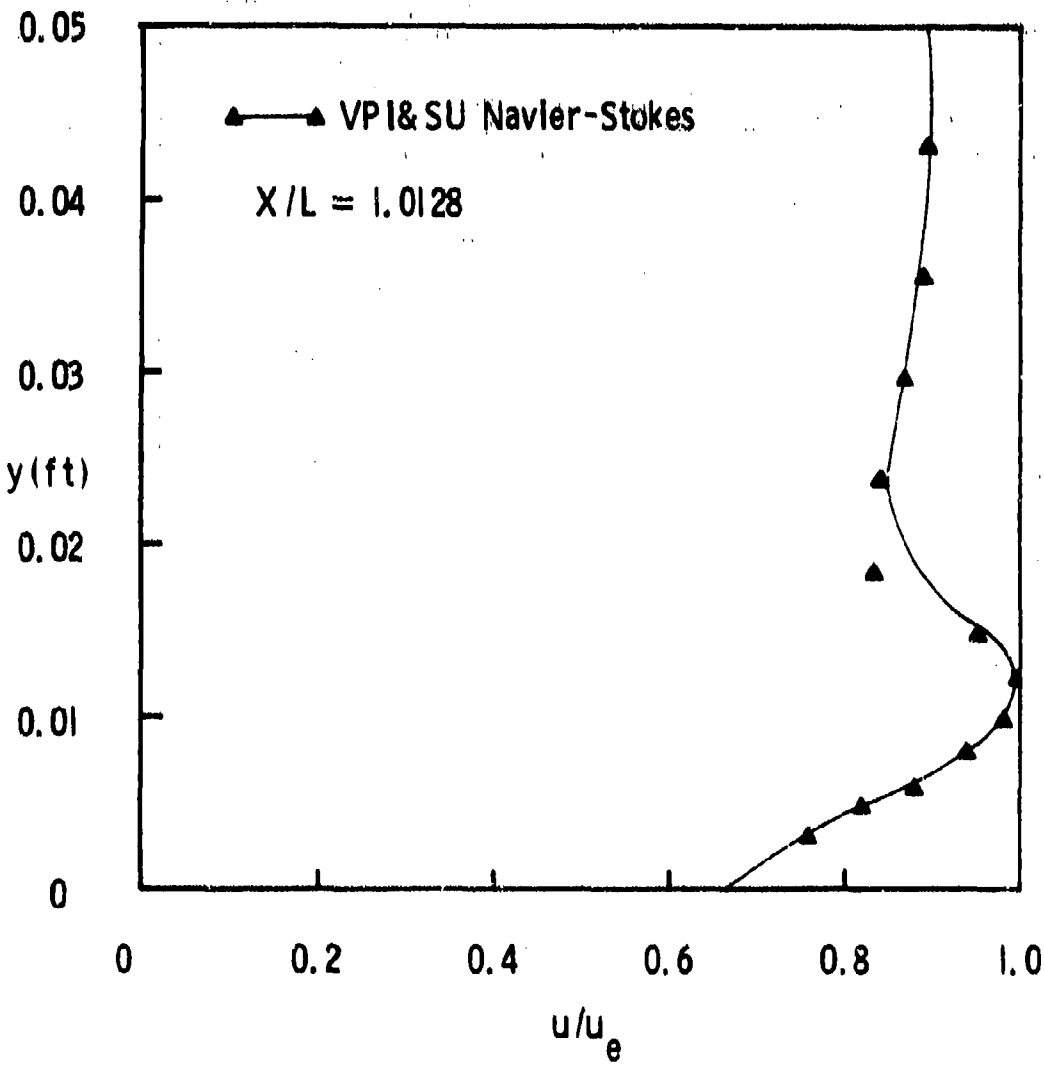

Fig. 37 Velocity profiles in the near wake (X/L = 1.0128) of test case 2 with a propeller in operation

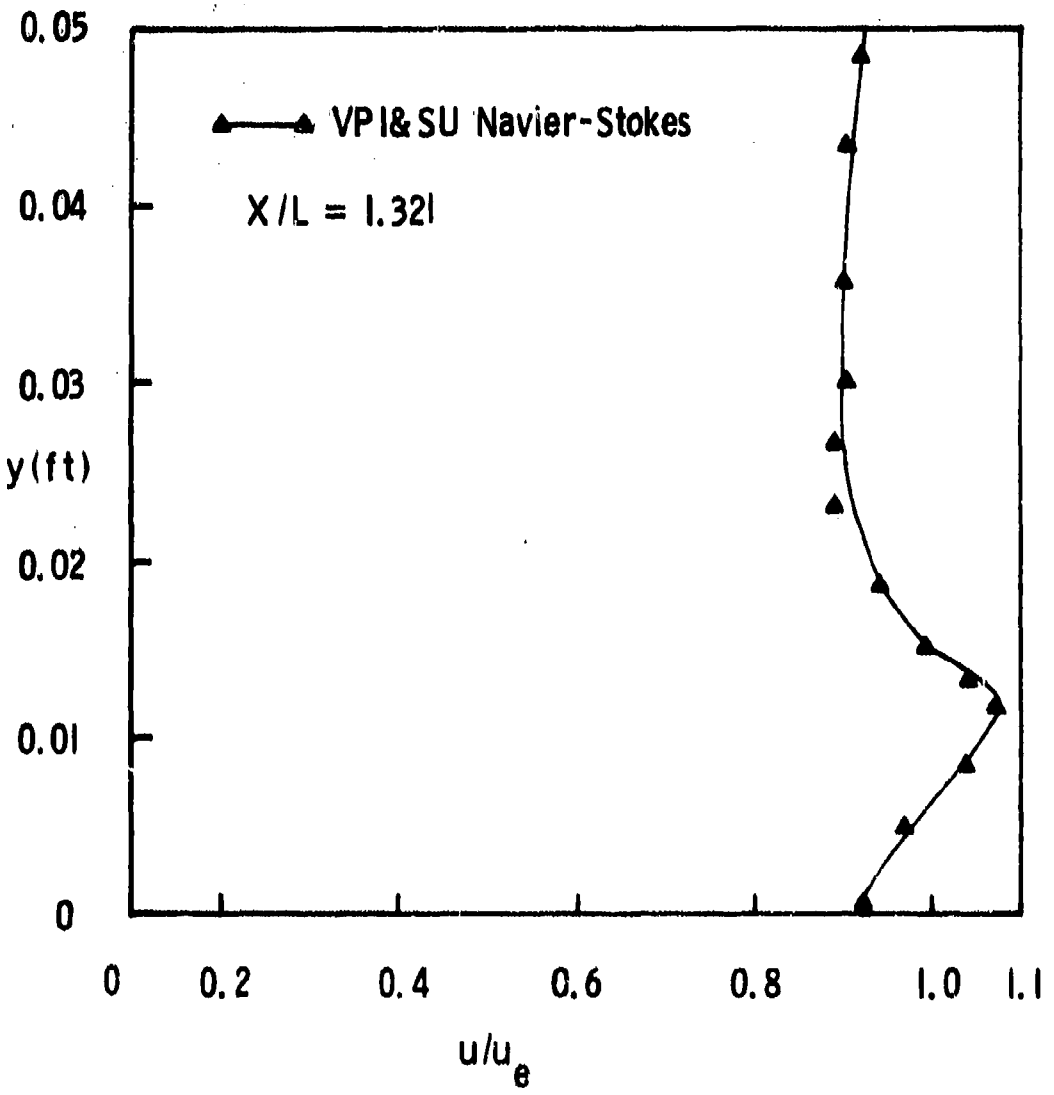

Fig. 38 Velocity profiles in the near wake (X/L = 1.321) of test case 2 with a propeller in operation